A PETROGRAPHIC STUDY OF CARBONATE PHASES IN THE ULTEN ZONE ULTRAMAFIC ROCKS: INSIGHTS INTO CARBONATION IN THE MANTLE WEDGE AND EXHUMATION-RELATED DECARBONATION

Bibiana Förster*,✉, Roberto Braga*, Sonja Aulbach, Deborah Lo Pò*, Giuseppe Maria Bargossi*** and **Volkmar Mair*****

* *Dipartimento di Scienze Biologiche, Geologiche ed Ambientali, Università di Bologna, Italy.*
** *Institut für Geowissenschaften, Goethe-Universität Frankfurt, Frankfurt am Main, Germany.*
*** *Autonome Provinz Bozen Südtirol, Amt für Geologie und Baustoffprüfung, Kardaun (BZ), Italy.*
✉ *Corresponding author, email: bibiana.forster2@unibo.it*

Keywords: *subduction zone processes, carbon cycle, carbonation of mantle wedge, carbonate phases, dedolomitization, mantle wedge peridotite, Ulten Zone.*

ABSTRACT

We present a comprehensive petrographic study on carbonates in orogenic mantle wedge-derived peridotites from the Ulten Zone (UZ) in the Eastern Italian Alps representing a fragment of the Variscan belt. These peridotites are found in ultramafic bodies incorporated in high-grade crustal rocks from a former continental slab and are characterized by highly variable mineral assemblages and microstructures, which reflect their evolution from spinel peridotite in a hot mantle wedge, to garnet peridotite after incorporation into the subducting slab and finally exhumation accompanied by retrogression. Carbonate phases in UZ peridotites are observed in diverse textural sites and can be related to particular petrographic peridotite types. Inclusions of dolomite and dolomite-breakdown products in primary spinel from coarse-grained protogranular peridotites indicate that carbon-bearing liquids were introduced into the mantle wedge at a time before achieving garnet stability. Discrete dolomite grains occur in fine-grained deformed garnet-bearing peridotite and are suggested to have formed simultaneously with hydrous phases (amphibole, apatite) from a carbon-bearing aqueous crustal slab-derived fluid during garnet stability. Intergrowths of calcite and brucite occur mainly in serpentinized fine-grained garnet-amphibole peridotites and are interpreted to be products of dedolomitization ($CaMg(CO_3)_2 + H_2O \rightarrow CaCO_3 + Mg(OH)_2 + CO_2$), thus decarbonation, during exhumation. Veins of dolomite and calcite-brucite indicate secondary dolomite formation from carbon-bearing fluids due to interaction with slab-derived crustal fluids during retrogression on the exhumation path of the UZ peridotite. Magnesite veins and calcite veins that are texturally linked to alteration features are probably of low-temperature origin. In summary, this petrographic study reveals multi-stage carbonation of the UZ peridotites during residence in the mantle wedge and decarbonation with the release of a carbon species during low-temperature peridotite reaction with aqueous fluids leading to serpentinization accompanied by dolomite breakdown, thus providing important constraints on the carbon budget and carbon cycling in collisional settings. Overall, the ubiquity of carbonates in a variety of textural settings in the UZ peridotites suggests that the supra-subduction zone mantle in continental settings represents an efficient carbon trap.

INTRODUCTION

In the debate of carbon transfer between Earth's reservoirs, the cycling of carbon between crust and mantle during subduction is of particular interest because carbon is effectively mobilized and recycled at active convergent margins (Poli, 2015 and references therein). Being largely incompatible in mantle silicate minerals (Shcheka et al., 2006), carbon in the mantle is commonly hosted by carbonate minerals, graphite and/or diamond as well as occurring in volatile carbon species, such as COH-fluids. Carbon may be introduced into peridotite mantle via, (1) the release of crust-derived C-bearing fluids at the slab-mantle interface during subduction (e.g., Bebout, 1996; Kerrick and Connolly, 1998; Molina and Poli, 2000; Scambelluri and Philippot, 2001; Poli et al., 2009) and/or, (2) the reaction of mantle peridotite with carbonated melts (e.g., Green and Wallace, 1988; Green et al., 1992; Ionov et al., 1993; 1996). Nevertheless, due to sparse natural record of carbonated peridotite samples, the nature of carbon transfer between crust and mantle remains little understood. Experimental studies reveal that carbonates in both hydrous and anhydrous mantle peridotites are stable in a broad temperature and pressure range (e.g., Wyllie and Huang, 1975; Eggler, 1978; Eggler et al., 1979; Tumiati et al., 2013), and several studies report the occurrence of carbonate minerals in mantle-derived ultramafic rocks (e.g., Ionov et al., 1993; 1996; 1998 and references therein; Zanetti et al., 1999; Lee et al., 2000; Laurora et al., 2001; Braga and Sapienza, 2007; Sapienza et al., 2009). However, for example, although mantle xenoliths have provided invaluable insights into the composition and evolution of the mantle, carbonate minerals can be destabilized during decompression upon entrainment in the host lava (Canil, 1990), largely excluding this sample type as a direct source of information on the deep carbon cycle. Experimental studies dealing with the stability of carbonate minerals at mantle conditions under appropriate oxygen fugacities revealed that carbonation of peridotite starts with the formation of dolomite + orthopyroxene at the expense of forsterite + clinopyroxene + CO_2 (Wyllie and Huang, 1975). In mantle peridotites, dolomite is stable at $P < 1.9$ GPa and at 900°C, followed by coexistent dolomite and magnesite up to 2.4 GPa and ultimately stability of magnesite at $P > 2.4$ GPa (Wyllie and Huang, 1975; Eggler et al., 1979; Tumiati et al., 2013). It has been shown that carbonate minerals are robust even at subduction zone conditions involving fluids and/or melts (Molina and Poli, 2000; Kerrick and Connolly, 2001). Decarbonation of peridotites occurs only at conditions of low pressures and high temperatures that are virtually not achieved along subduction geotherms (Tumiati et al., 2013), but exhumation on a clockwise retrograde P-T path is considered to prompt decarbonation and CO_2-degassing of formerly subducted carbonate-bearing rocks (Kerrick and Connolly, 1998). It is becoming increasingly clear, however, that mantle carbonates

are soluble as ionic species in aqueous fluids and in carbonatitic liquids under P-T conditions applicable to subduction zones, thus helping to redress the discrepancy between observed carbon inputs and outputs in subduction zones that arises if only decarbonation reactions are considered (Frezzotti et al., 2011; Manning et al., 2013; Ague and Nicolescu, 2014; Facq et al., 2014; Poli, 2015; Ferrando et al., 2017). Orogenic carbonate-bearing mantle peridotites can provide important constraints on the nature and effects of subduction-related fluids and melts on the trapping and remobilization of carbon during collisional tectonics.

In this paper we present a comprehensive petrographic study on the occurrence of diverse carbonate minerals in orogenic peridotites and pyroxenites from the Ulten Zone (UZ) tectonic unit in the Eastern Italian Alps (Fig. 1). These peridotites derive from a supra-subduction zone mantle wedge being affected by various petrologic processes involving metasomatic agents during subduction and exhumation (Scambelluri et al., 2006; Tumiati et al., 2007). Several previous studies (Obata and Morten, 1987; Godard et al., 1996; Braga and Sapienza, 2007; Marocchi et al., 2009; Sapienza et al., 2009; Malaspina and Tumiati, 2012) reported the occurrence of dolomite in different textural sites in the UZ peridotites, the precipitation of which has been suggested to be prompted by infiltration of C-bearing metasomatic aqueous fluids at different depths along the interface between the subducting continental slab and the overlying mantle wedge (Rampone and Morten, 2001; Sapienza et al., 2009). Here, we present new and extended petrographic evidence of carbonate minerals and especially the occurrence of dedolomitization products in wedge-derived peridotite mantle, which have not been described previously. As we will show, different carbonate minerals in these rocks were precipitated during different stages of the subduction-exhumation cycle. In addition, their occurrence in a variety of textural settings, from discrete grains to veins, attests to the mobilization and "fixation" of carbon. Hence, the UZ peridotites are a promising natural laboratory to study carbon cycling in orogenic settings. We will discuss the presence of carbonate minerals and dolomite-breakdown products in the context of the complex tectono-metamorphic evolution of the UZ and we will link our petrographic observations to known carbonate stability at conditions occurring in crust and mantle in collisional subduction zone settings.

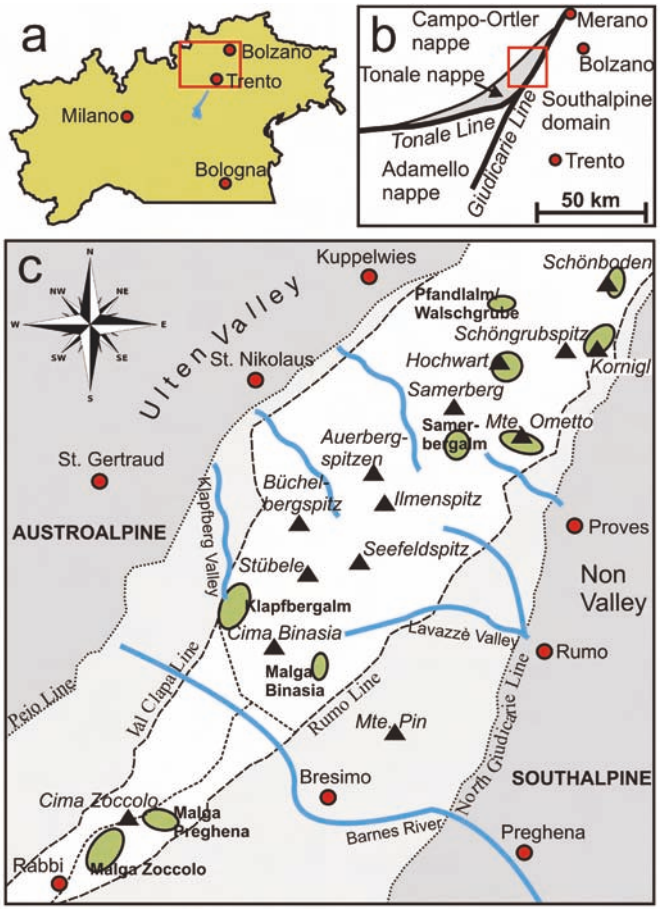

Fig. 1 - Map of the Ulten Zone tectonic unit. (a) Rectangle marks the location of the Ulten Zone in the Alps in North Italy; (b) Rectangle marks the location of the Ulten Zone in the Tonale nappe as a fragment of the Paleozoic Variscan belt; (c) White field encompasses the Ulten Zone located between the Val Clapa Line and the Rumo Line. Ellipses mark the locations of the ultramafic bodies from which peridotite samples were selected for this study.

Geologic background and previous work

The Ulten Zone (UZ) tectonic unit (e.g., Morten et al., 1976; Martin et al., 1993; 1998) outcrops in the Nonsberg mountain range located between the Ulten Valley and Non Valley in the Eastern Alps in Italy (Fig. 1). The orogenic UZ represents a fragment of the Late Paleozoic Variscan belt (Fig. 1b; Godard et al., 1996) and consists of foliated high-grade metamorphic crustal basement (garnet-kyanite paragneiss, migmatite and granitic to tonalitic orthogneiss; Obata and Morten, 1987; Godard et al., 1996; Martin et al., 1998) and bodies of ultramafic rocks (peridotite ± pyroxenites; Morten and Obata, 1983; Obata and Morten, 1987; Godard et al., 1996 and references therein). These numerous peridotite bodies are exposed at the surface as lenses of variable sizes (usually a few meters thick and up to hundreds of meters length) included within the crustal metamorphic basement. The contact zones between the crustal rocks and the peridotite lenses are usually sharp but rarely exposed at the surface (Obata and Morten, 1987). The UZ peridotites have been interpreted to represent slices of a Late Paleozoic supra-subduction zone mantle wedge that were incorporated in a subducting continental slab (Godard et al., 1996; Nimis and Morten, 2000) and subsequently exhumed during the Variscan orogeny (Godard et al., 1996). Ulten Zone peridotites display a transition from coarse-grained (up to a few cm) spinel-peridotites via a transitional type to highly deformed fine-grained (0.2 mm to 1 mm) garnet-amphibole peridotites and amphibole-chlorite peridotites (Obata and Morten, 1987). The transitional type is a porphyroclastic garnet-bearing peridotite with large orthopyroxene and olivine in a granoblastic-polygonal matrix. The highly variable petrographic occurrences have been interpreted to record several processes during the complex tectono-metamorphic UZ history. Recent studies suggest the following evolutionary stages: (1) Coarse-grained protogranular spinel-lherzolite predominantly constituted the initial lithotype in the mantle wedge (Obata and Morten, 1987), residing at high temperatures (> 1100°C) and moderate pressure (~ 1.5 GPa; Nimis and Morten, 2000). At this early, pre-Variscan stage, the peridotites were infiltrated by hot (> 1400°C) melts derived from deeper levels of the mantle wedge (Nimis and Morten, 2000; Scambelluri et al., 2006; Marocchi et al., 2007), enabling the crystallization of pyroxenitic segregates (Nimis and Morten, 2000). (2) While flowing towards the continental subducting slab via corner flow,

the peridotites underwent isobaric cooling (down to ~ 850°C), followed by transport to greater depths (corresponding to pressures of 2.0 to 2.5 GPa) close to the slab-wedge interface (Obata and Morten, 1987; Nimis and Morten, 2000). Due to the high-pressure eclogite-facies conditions and the infiltration of slab-derived aqueous fluids at this stage, coarse spinel peridotites were re-crystallized into amphibole ± garnet-bearing assemblages (Rampone and Morten, 2001; Scambelluri et al., 2006; Marocchi et al., 2007; Tumiati et al., 2007). Two hypotheses have been suggested for the subsequent metamorphic path: (a) incorporation of peridotites into the continental slab and subduction on a common prograde P-T path to peak metamorphic conditions (~ 2.7 GPa and ~ 850°C; Nimis and Morten, 2000), accompanied by the transformation into garnet-amphibole peridotite; (b) the peridotites reside in the mantle wedge and are infiltrated by crust-derived aqueous fluids while the slab reaches peak metamorphic conditions, followed by emplacement of peridotites during exhumation of crustal rocks; (3) In both cases peridotites and crustal rocks would start a common exhumation path at ca. 330 Ma (Tumiati et al., 2003). The Late Paleozoic exhumation, mylonitic deformation and retrograde overprint into fine-grained porphyroclastic garnet-amphibole peridotite (Obata and Morten, 1987; Scambelluri et al., 2006) is evidenced by the occurrence of kelyphites overgrowing the deformed textures (Godard and Martin, 2000) and this marks the latest Variscan stage of the UZ evolution. Since the UZ was only slightly overprinted by Alpine metamorphism, the UZ lithologies preserve pre-Alpine metamorphic signatures and assemblages (Godard et al., 1996; Hauzenberger et al., 1996).

Sample materials and petrographic analytical methods

The Ulten Zone peridotites described in this study largely derive from a new sample set including samples from localities widespread across the whole UZ tectonic unit, including localities that were not previously studied (Table 1; Fig. 1c). The sampled ultramafic bodies consist of peridotites ± pyroxenitic rocks and allowed targeted sampling of, in general, well-preserved outcrops without visible weathering. The chosen specimens are representative of all macroscopically detectable petrographic characteristics in each sample locality.

Polished thick sections (~ 100 μm) of samples of the new sample set were analyzed using an optical transmitted light microscope and an energy dispersive (EDS) scanning electron microscope (SEM; Philips 515B, 5 μm spot size, 15 kV voltage) at the University of Bologna (Italy) as well as a Phenom XL SEM (15 kV voltage) at Lehigh University (USA). The latter allows detection of the volatile elements carbon and oxygen and was, therefore, used to distinguish carbonate and oxide phases and for the generation of element maps. The petrographic observations of the Hochwart sample set were also carried out with polarizing optical microscopy and electron imaging at the University of Bologna as well as with a JEOL Superprobe 8100 at the Institute of Mineralogy and Petrography, University of Innsbruck (Austria).

Table 1 summarizes the provenance and petrographic characteristics of the studied peridotite samples as well as the occurrences of different carbonate phases in theses samples. For the petrographic description of the Ulten Zone peridotites we use the petrographic terms "coarse-grained" and "fine-grained" peridotites corresponding to the terms "coarse-type" and "fine-type" introduced by Obata and Morten (1987). The coarse-grained type is mostly relatively undeformed spinel lherzolite and composed of (in decreasing modal abundance order) olivine + orthopyroxene + clinopyroxene + spinel ± garnet with texture ranging from protogranular to porphyroclastic. If garnet is present, spinel is rimmed by garnet, which in turn is rimmed by a kelyphitic corona (Godard and Martin, 2000). The fine-grained type reveals various metamorphic textures, from porphyroclastic to tabular or mosaic equigranular. The main mineral assemblage is composed of olivine + orthopyroxene + pale-green amphibole + garnet + spinel ± clinopyroxene. In this fine-type peridotite, garnet is locally completely transformed into aggregates consisting of kelyphites (amphibole + pyroxenes ± spinel). The serpentinization degree of the fine-grained peridotite ranges from virtually absent to strongly serpentinized. According to Obata and Morten (1987), peridotites of the fine-grained type are much more abundant than the coarse-grained peridotites of the Ulten Zone. Indeed, while fine-grained spinel-peridotites occur in all newly studied localities (n = 9, exclusive Hochwart), coarse-grained spinel-peridotite was found in only six of the sampled peridotite bodies. In those exposures coarse-grained undeformed peridotite often occurs as "lenses" within the fine-grained peridotite that reveals mylonitic deformation (Fig. 2).

CARBONATES IN ULTEN ZONE PERIDOTITES

Dolomite

Previous studies report consistently the occurrence of dolomite in diverse structural sites of fine-grained garnet-amphibole peridotites of the UZ: as inclusions in garnet (Obata and Morten, 1987; Godard et al., 1996); in the peridotite matrix, as large cm-sized grains (Obata and Morten, 1987; Marocchi et al., 2009) or porphyroclasts (Sapienza et al., 2009); and as interstitial µm-sized grains disseminated within the recrystallized foliated peridotite matrix (Godard et al., 1996; Braga and Sapienza, 2007; Sapienza et al., 2009). The observed dolomites commonly coexist and/or are in contact with apatite grains, regardless their microstructural site. These reports are consistent with our observation that interstitial disseminated matrix dolomite grains occur only in fine-grained porphyroclastic mylonitic garnet-amphibole peridotites (Fig. 3) and in similar samples containing garnet pseudormorphs

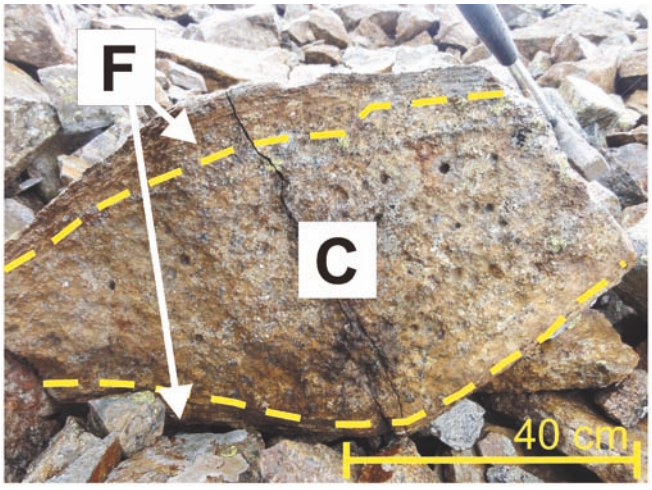

Fig. 2 - Photograph of an Ulten Zone peridotite block from Malga Binasia consisting of a coarse-grained peridotite lens (C) embedded in fine-grained mylonitic deformed peridotite (F). The coarse lens was largely excluded from hydration and shearing.

Table 1 - Petrographic description of Ulten Zone peridotites from different localities, with particular attention to their carbonate content.

Sample/textural type	Locality	Texture	Carbonates	Apatite	Serpent.[1]	Comments
Coarse-grained						
Ko2a	Kornigl	transitional from protogranular to porphyroclastic	Cal veins	-	yes	
KoD4	Kornigl	transitional from protogranular to porphyroclastic	Mgs vein	-	yes	
MBS1	Malga Binasia	transitional from protogranular to porphyroclastic	Cal veins, cal veins in cpx	-	yes	
MBS2	Malga Binasia	protogranular-granoblastic	Cal(+dol) veins, ± cal-brc	-	little	
MOL1.5	Monte Ometto	protogranular-granoblastic + fine-grained recrystallized parts	Mgs vein, interstitial dol + mgs, dol crystal in amp vein	-	-	
MZS1.2	Malga Zoccolo	protogranular-granoblastic + fine-grained recrystallized parts	Cal veins, cal veins in cpx	-	yes	
PL1.1	Malga Preghena	protogranular-granoblastic + fine-grained recrystallized parts	Cal veins, cal veins in spl	-	yes	
PRE-A	Malga Preghena	protogranular-granoblastic + fine-grained recrystallized parts	Cal veins, cal veins in cpx	-	yes	
Fine-grained (grt-free)						
KL1.7-2	Klapfbergalm	granoblastic-porphyroclastic, mylonitic	Cal veins	-	yes	blasts of kely/amp/chl after grt
KL1-3a	Klapfbergalm	granoblastic-porphyroclastic, mylonitic	Cal-brc	yes	yes	blasts of kely/amp/chl after grt
KL2.2	Klapfbergalm	granoblastic, mylonitic	Cal-brc	?	yes	highly amphibolized, blasts of kely/amp/chl after grt
Ko2b, Ko2c	Kornigl	granoblastic-porphyroclastic, mylonitic	Cal veins, cal veins in amp	?	yes	
KoD9	Kornigl	granoblastic-porphyroclastic, mylonitic	Mgs vein	?	yes	highly amphibolized
KoDb2 (medium-grained)	Kornigl	transitional from protogranular to porphyroclastic	Cal-brc vein, cal veins, cal veins in cpx and spl	?	yes	blasts of kely/amp/chl after grt
MBS3TZ	Malga Binasia	granoblastic-porphyroclastic, mylonitic	Cal vein	?	yes	highly amphibolized, blasts of kely/amp/chl after grt
MR141B	Samerbergalm	granoblastic-porphyroclastic, mylonitic	Dol grains in serpentine vein	?	yes	
SBB2F	Schönboden	granoblastic-porphyroclastic, mylonitic	Dol crystal related to mgs aggregate, mgs veins, dol veinlets, cal veinlets	yes	yes	
Fine-grained grt-bearing						
KBA8	Klapfbergalm	granoblastic-porphyroclastic, mylonitic	Cal-brc, cal-brc in grt, cal+srp in grt, cal veins in grt, cal veins	?	little	
KL1.2-3	Klapfbergalm	granoblastic-porphyroclastic, mylonitic	Cal-brc, dol grains in matrix, dol in ap	yes	little	
KL1.3c	Klapfbergalm	granoblastic-porphyroclastic, mylonitic	Cal-brc	yes	little	
KL1.6	Klapfbergalm	granoblastic-porphyroclastic, mylonitic	Dol vein + cal-brc	yes	little	
KL2.4-2b	Klapfbergalm	granoblastic-porphyroclastic, mylonitic	Cal-brc, dol in spl in grt, cal-brc in ms incl. in spl	?	yes	
PL1-6	Malga Preghena	granoblastic-porphyroclastic, mylonitic	Cal-brc	?	yes	
PL1-9	Malga Preghena	granoblastic-porphyroclastic, mylonitic	Cal-brc, cal-brc in ms incl. in spl, cal+srp in ms incl. in spl, cal veins	yes	yes	
SB2-1	Schönboden	granoblastic-porphyroclastic, mylonitic	Cal-brc, cal veins	?	yes	
SB2-2	Schönboden	granoblastic-porphyroclastic, mylonitic	Cal-brc, cal-brc veinlet, cal(+dol) veins	yes	yes	
SB3-1	Schönboden	granoblastic-porphyroclastic, mylonitic	Cal-brc, cal veins, cal veins in amp and grt	yes	yes	
SB3-2	Schönboden	granoblastic-porphyroclastic, mylonitic	Cal-brc, cal(+dol) veins, dol in serpentinized parts, cal veins in amp and grt	yes	yes	
SB3-3	Schönboden	granoblastic-porphyroclastic, mylonitic	Cal-brc, cal veins	?	yes	
SB3-4	Schönboden	granoblastic-porphyroclastic, mylonitic	Dol in ol, cal veins	-	yes	
SBA4	Samerbergalm	granoblastic-porphyroclastic, mylonitic	Dol grains in matrix	yes	-	
SBA5	Samerbergalm	granoblastic-porphyroclastic, mylonitic	Dol grains in matrix, dol in amp and ol	yes	-	
SBA7	Samerbergalm	granoblastic-porphyroclastic, mylonitic	Dol grains in matrix, dol in ol	yes	-	
VM25P10A	Hochwart	granoblastic-porphyroclastic, mylonitic	Dol grains in matrix, dol in amp and zrn, dol in grt pseudomorph	yes	little	
VM25P10B	Hochwart	granoblastic-porphyroclastic, mylonitic	Dol in amp coronas around grt, part of ms incl. in grt, band of interstinal dol	yes	-	
VM25P10C	Hochwart	granoblastic-porphyroclastic, mylonitic	Dol grains in matrix, dol in amp, dol in kely around grt, dol in serpentinized parts	?	little	
VM25P11	Hochwart	granoblastic-porphyroclastic, mylonitic	Dol grains in matrix, dol in amp and ol, dol as part of grt pseudomorph, polycrystalline dol aggregate, dol in serpentinized parts	yes	little	
WG1	Walschgrube	granoblastic-porphyroclastic, mylonitic	Cal-brc, cal+dol veins, dol in serpentinized parts	yes	yes	
WG2	Walschgrube	granoblastic-porphyroclastic, mylonitic	Cal-brc, cal veins	yes	yes	
WG7	Walschgrube	granoblastic-porphyroclastic, mylonitic	Cal-brc, cal-brc in spl in grt, cal-brc in grt	yes	yes	highly amphibolized, veins of fibrous amp
WG9b, WG9c	Walschgrube	granoblastic-porphyroclastic, mylonitic	Cal-brc, cal-brc in ms incl. in spl, cal veins	?	yes	

[1]Serpent.: serpentinization

Mineral abbreviations after Whitney and Evans (2010): Cal: calcite; mgs: magnesite; brc: brucite; dol: dolomite; amp: amphibole; grt: garnet; ol: olivine; cpx: clinopyroxene; spl: spinel; srp: serpentine; ap: apatite; chl: chlorite

Other abbreviations: kely: kelyphite; ms incl.: multi-phase solid inclusion

(Table 2). These peridotites are largely non-serpentinized and garnets occasionally have kelyphite coronas. Dolomite grains are often in contact with apatite (Fig. 3a, b) and amphibole (Fig. 3c), as well as with garnet (kelyphite-free; Fig. 3c, d). In some of these samples and in other fine-grained garnet-amphibole peridotites, dolomite occurs also as inclusions in matrix apatite (Fig. 4a), amphibole (Fig. 4b) and olivine (Fig. 4c). In one sample, dolomite is associated with apatite as lobate inclusions in a coarse zircon crystal (~ 1 cm length; Fig. 4d). Also, dolomite occurs as part of multi-phase solid inclusions (Fig. 4e) in coarse garnet (~ 2 cm length) with a kelyphitic corona consisting of amphibole-pyroxene symplectites. Observed dolomite-bearing mineral associations in these multi-phase solid inclusions are dolomite ± spinel ± chlorite and amphibole + dolomite + sulfide ± calcite ± dissakisite ± apatite ± spinel ± chlorite ± sapphirine, whereas dolomite-free mineral associations comprise amphibole + apatite + phlogopite + spinel + sulfide. Such multi-phase solid inclusions represent former entrapped fluid inclusions, as described by Frezzotti and Ferrando (2015). In samples with retrogressed garnet, dolomite occurs in a garnet pseudomorph together with amphibole and spinel (Fig. 5a), in contact with kelyphite around garnet, as part of pseudomorphs after garnet together with kelyphite, calcite and chlorite and in spinel-free amphibole coronas together with orthopyroxene around garnet. Occasionally, aggregates of dolomite form bands (vein-like?) and occur in contact with amphibole with curvilinear to embayed contacts to the matrix minerals (Fig. 5b-d). It rarely appears that dolomite veins contain patches of calcite-brucite intergrowths (next chapter). A lenticular polycrystalline aggregate of dolomite (~ 5 cm in length; Fig. 6a) in one sample is composed of randomly oriented crystals with an average grain size of 500 μm which decreases towards the aggregate rim. Apatite is commonly located between the dolomite and the matrix (Fig. 6b, c); the dolomite aggregate hosts coarse amphibole enclosing spinel, sulfides and fracture-filling dolomite. Dolomite in the little-serpentinized garnet-amphibole peridotites may also occur as grains with frayed boundaries located within rare serpentine veins crosscutting the matrix.

In (highly-)serpentinized fine-grained garnet-bearing samples, fine veinlets (~ 10 μm) consisting of dolomite associated with magnetite ± calcite ± (secondary?) serpentine(/chlorite?) crosscut the pre-existing serpentine mesh texture (Fig. 7a). Future chemical analyses will resolve the presence of serpentine vs. chlorite. A highly-serpentinized fine-grained garnet-free peridotite contains a distinct secondary serpentine vein (~ 3 mm thickness) containing dolomite grains with frayed grain boundaries (Fig. 7b). In other samples, rare dolomite grains occur within the serpentine mesh texture

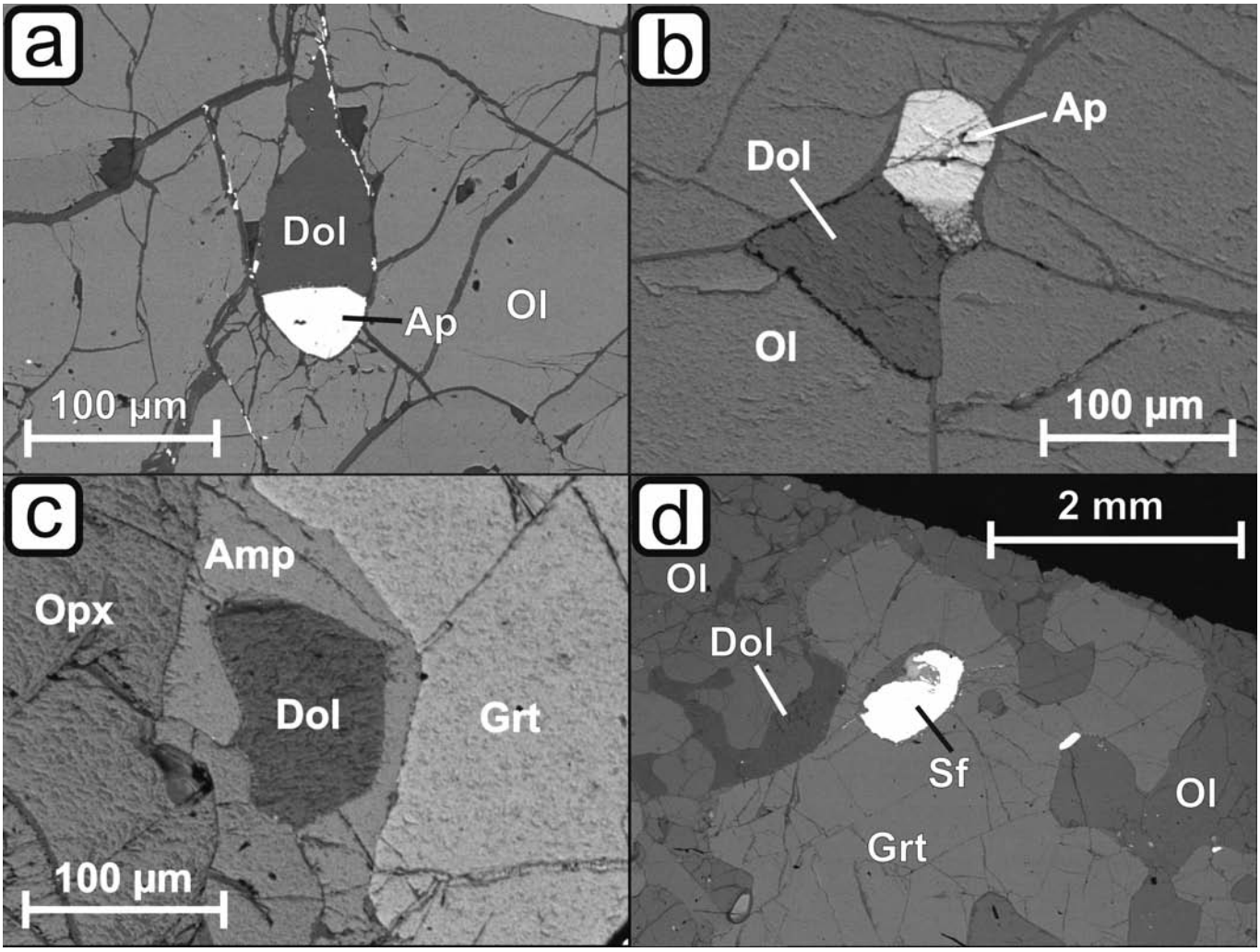

Fig. 3 - Back-scattered electron images of sections showing discrete dolomite grains in the matrix of non-serpentinized fine-grained garnet-amphibole peridotites associated with (a, b) apatite (samples KL1.2-3 and SBA4); (c, d) amphibole and garnet (SBA7). Mineral abbreviations after Whitney and Evans (2010), sf- sulfide.

Table 2 - Summary of various carbonate phases and their textural setting in different microstructural types of Ulten Zone peridotites.

Textural type / sample names	Carbonate phase						
	Interstitial dolomite	Dolomite inclusions	Dolomite veins	Grains / patches of calcite-brucite intergrowths	Inclusions of calcite-brucite intergrowths	Calcite veins	Magnesite
Coarse-grained protogranular							
MOL1.5	Anhedral with curvilinear grain boundaries in contact with silicate minerals, spatially related with amp, partly associated with mgs (Fig. 5e,f)						Distinct vein (≈500 µm in thickness) with frayed grain boundaries
Ko2a, MBS1, MBS2, MZS1.2, PL1.1, PRE-A						Associated with srp veins (Fig. 11c)	
MBS1, MZS1.2, PRE-A						Crosscutting cpx	
MBS2			Associated with mag ± cal ± (secondary) srp(/chl?) crosscutting pre-existing srp mesh texture	Rarely in srp mesh texture			
Ko2c						Crosscutting amp	
PL1.1						Crosscutting spl (Fig. 11d)	
KoD4							Veins, associated with srp veins (Fig. 11f)
Fine-grained non-serpentinized grt-amp peridotites							
SBA4, SBA5, SBA7, KL1.2-3, VM25P10C, VM25P11	Disseminated in matrix, often associated with ap, amp, grt (Fig. 3)						
KL1.2-3		In ap (Fig. 4a)					
SBA5, VM25P10C, VM25P11		In amp (Fig. 4b)					
SBA5, SBA7, VM25P11		In ol (Fig. 4c)					
VM25P10B	In spl-free amp coronas around grt together with opx; in band (vein-like?) in textural association with amp (Fig. 5b)	Part of multi-phase solid inclusion in coarse grt (Fig. 4e)					
VM25P10C	In contact with kely around grt; with frayed boundaries located within srp veins crosscutting the matrix						
VM25P11	Part of grt pseudomorph together with kely, cal, chl; lenticular polycrystalline aggregate (≈5 cm in length; Fig. 6a); located within rare srp veins crosscutting the matrix						
KL1.6			Consisting of aggregates of interstitial anhedral dol (up to 400 µm) crosscutting the peridotite matrix; partly texturally associated with amp (Fig. 5c,d), contains patches of cal-brc intergrowths	Situated within dol vein (Fig. 5c,d)			
Fine-grained non-serpentinized amp-bearing peridotite with grt pseudomorphs							
VM25P10A	Disseminated in matrix; together with amp and spl as grt pseudomorph (Fig. 5a)	In amp (Fig. 4b); anhedral with curvilinear boundaries spatially associated with ap as lobate inclusion in zrn (Fig. 4d)					
Fine-grained serpentinized grt-amp peridotites							

Mineral abbreviations after Whitney and Evans (2010)

Table 2 (*continued*)

Textural type / sample names	**Carbonate phase**						
	Interstitial dolomite	*Dolomite inclusions*	*Dolomite veins*	*Grains / patches of calcite-brucite intergrowths*	*Inclusions of calcite-brucite intergrowths*	*Calcite veins*	*Magnesite*
KBA8, KL1.3c, KL2.4-2b, PL1.6, PL1.9, SB2-1, SB2-2, SB3-1, SB3-2, SB3-3, WG1, WG2, WG7, WG9b, WG9c				With frayed boundaries, commonly located within serpentinized parts of the peridotites, often contoured by Fe-oxide and often textural relation to cal veinlets (Fig. 9a-f)			
SB3-2, WG1	Rarely, situated within srp mesh texture (Fig. 7c)						
SB2-2, SB3-2, WG1,			Associated with mag ± cal ± (secondary) srp(/chl?) crosscutting pre-existing srp mesh texture (Fig. 7a)				
KBA8, SB3-1, SB3-2						Crosscutting amp and grt	
KBA8, SB2-1, SB2-2, SB3-1, SB3-2, SB3-4, WG1, WG2, WG9b, WG9c						Associated with srp veins (Fig. 11c)	
SB3-4		In ol (Fig. 4f)					
KL2.4-2b		In spl hosted in grt (Fig. 8a)					
KL2.4-2b, PL1.9, WG9b					Part of multi-phase solid inclusion in spl (Fig. 8c)		
WG7					In spl hosted in grt (Fig. 8b)		
KBA8, WG7					In grt, occasionally touching spl and/or related to srp (Fig. 8d,e)		
KBA8, PL1.9						Cal + srp intergrowths hosted in grt, related to srp vein and as part of multi-phase solid inclusion in spl	
Fine-grained serpentinized peridotite							
MR141B	Situated in secondary srp vein (≈3 mm in thickness, Fig. 7b)						
SBB2F	Well-preserved idiomorphic crystal (~150 µm in length), texturally closely related with mgs aggregate, which is crosscut by thin dol veinlets (≈10 µm, Fig. 7d-f)						Aggregate with rippled grain boundaries, closely related to dol grain, residing within secondary srp (Fig. 7d-f); veins situated within srp veins
KL1.3a, KL2.2, KoDb2				Grains with frayed boundaries, commonly located within serpentinized parts of the peridotites, often contoured by Fe-oxide and often textural relation to cal veinlets (Fig. 9a-f)			
KoDb2				Vein (≈150 µm in thickness) located within srp vein, crosscutting peridotite matrix, interlaced with srp and mag (Fig. 11a,b)		Crosscutting cpx and spl (Fig. 11d)	
KL1.7-2, Ko2b, Ko2c, KoDb2, MBS3TZ, SBB2F						Associated with srp veins (Fig. 11c)	
KoD9							Distinct vein with frayed grain boundaries (≈2 mm in thickness, Fig. 11e)

Mineral abbreviations after Whitney and Evans (2010)

(Fig. 7c) that replaces the primary ultramafic mineral assemblage. In one fine-grained porphyroclastic mylonitic sample, a well-preserved idiomorphic dolomite crystal (~ 150 μm length) and a magnesite aggregate with rippled grain boundaries are in textural equilibrium, residing within the serpentine mesh that replaces the primary ultramafic mineral assemblage (Fig. 7d-f). The magnesite aggregate is crosscut by thin (~ 10 μm) dolomite veinlets which do not occur in the surrounding serpentine (Fig. 7d-f). The different shades of the dolomite crystal (black) and the dolomite veins (gray) in

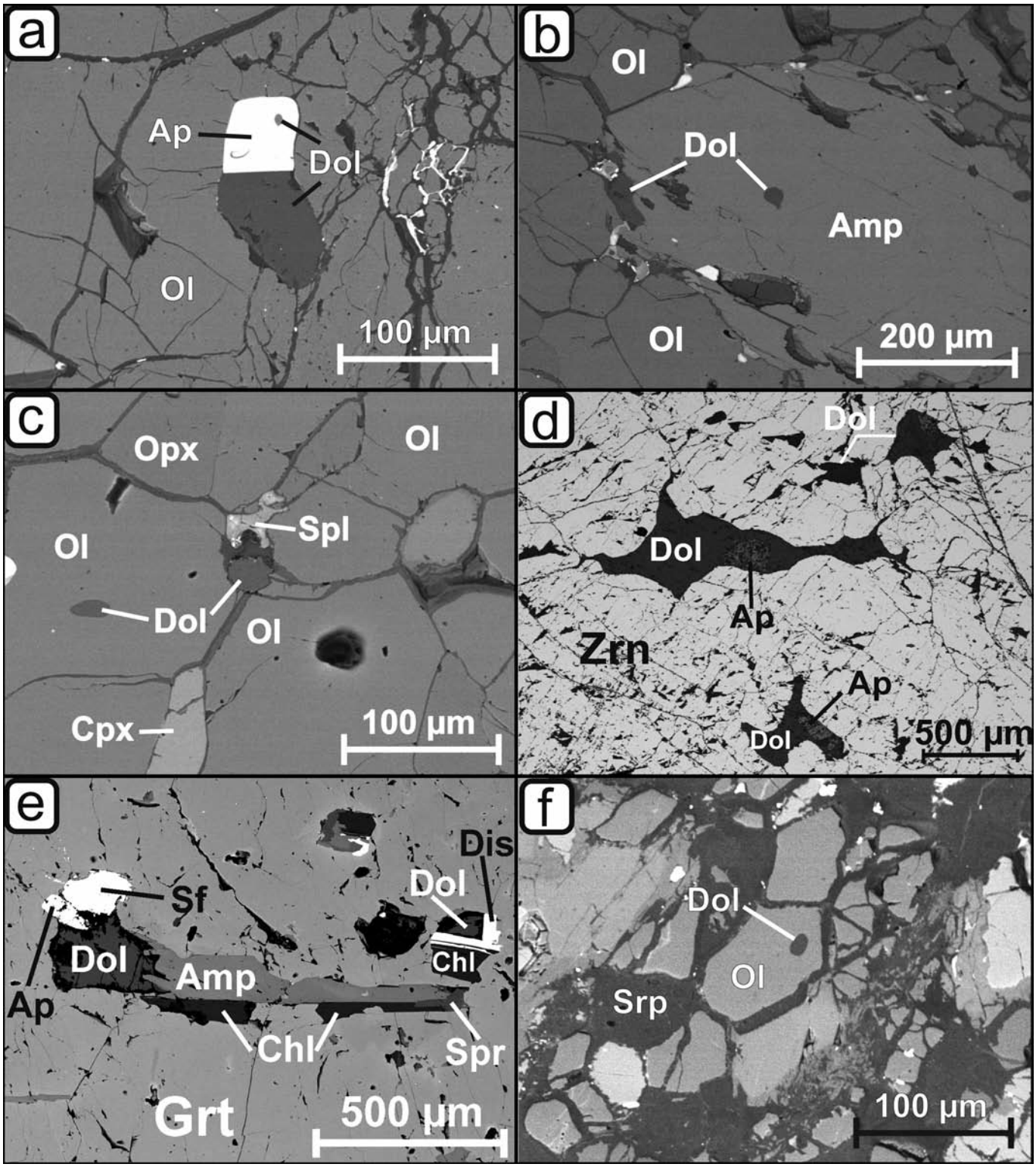

Fig. 4 - Back-scattered electron images of dolomite inclusions in (a) apatite (KL1.2-3); (b) amphibole (SBA5); (c) olivine (SBA5) in the matrix of non-serpentinized fine-grained garnet-amphibole peridotites; (d) lobate inclusions of anhedral dolomite with curvilinear grain boundaries in zircon crystal (~ 1 cm length) in a fine-grained garnet-amphibole peridotite (VM25P10A); (e) dolomite as part of a multi-phase solid inclusion in a coarse garnet (~ 2 cm length) surrounded by a kelyphitic corona (VM25P10B); (f) dolomite inclusion in olivine located in the serpentine mesh texture in a serpentinized fine-grained garnet-amphibole peridotite (SB3-4). Mineral abbreviations after Whitney and Evans (2010), sf- sulfide, dis- dissakisite.

Fig. 7d indicate two different dolomite generations with different chemical compositions. In other serpentinized fine-grained garnet-amphibole peridotites, dolomite occurs as an inclusion in matrix olivine (Fig. 4f) and as a euhedral inclusion in spinel hosted in garnet (Fig. 8a).

In one coarse-grained protogranular sample, which also contains a distinct magnesite vein, interstitial anhedral dolomite with curvilinear grain boundaries in contact with the silicate minerals is highly abundant (Fig. 5e, f) and spatially associated with amphibole. So far, this is the first

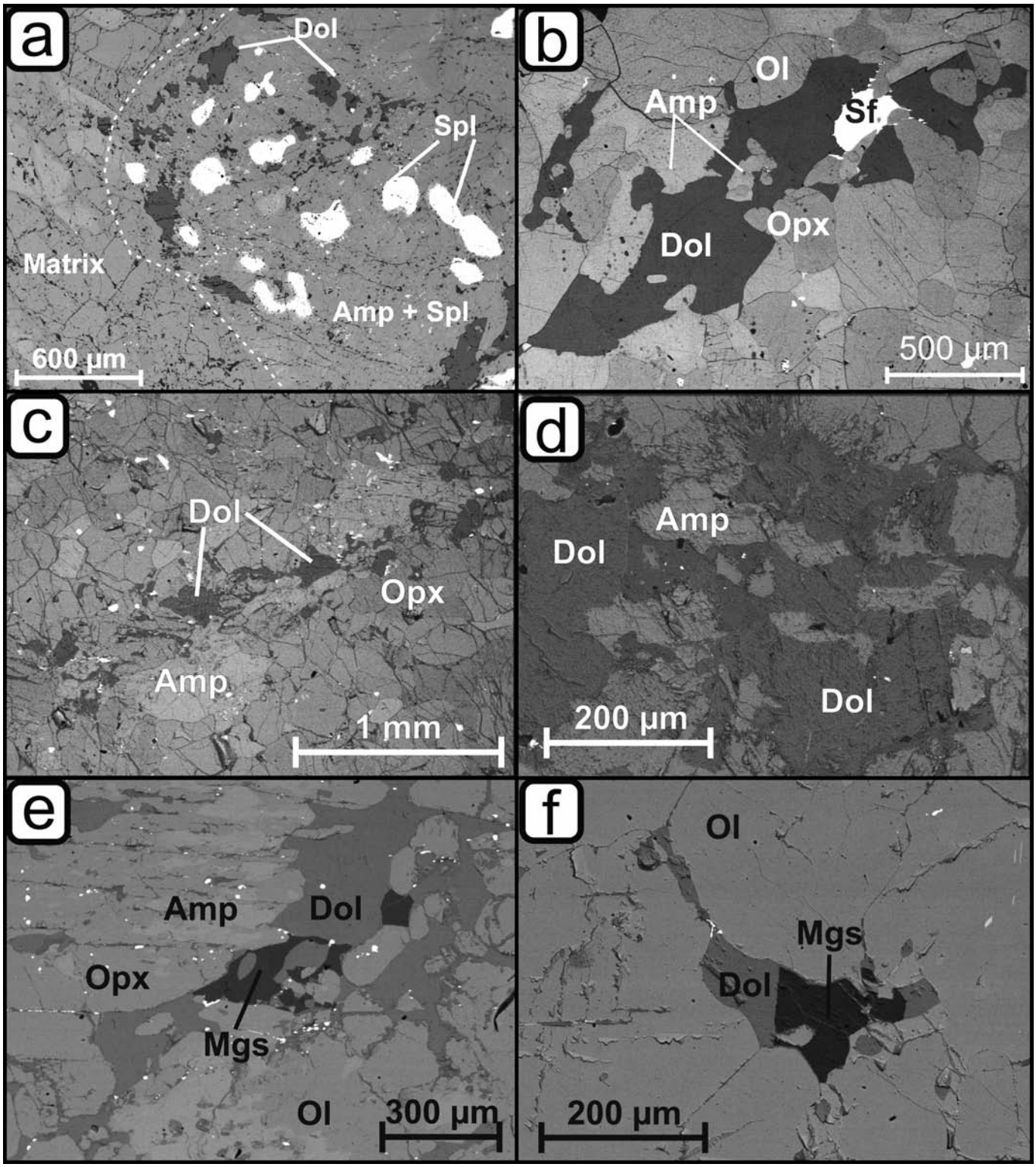

Fig. 5 - Back-scattered electron images of (a) dolomite in retrogressed garnet associated with spinel and amphibole in a fine-grained garnet-amphibole peridotite (VM25P10A); (b-d) bands/veins of dolomite associated with amphibole in fine-grained garnet-amphibole peridotites, dolomite has curvilinear contacts to the matrix minerals, in (b) sample VM25P10B and (c, d) sample KL1.6; (e, f) interstitial anhedral dolomite grains associated with magnesite with curvilinear contacts to matrix minerals in coarse-grained protogranular peridotite MOL1.5. Mineral abbreviations after Whitney and Evans (2010), sf- sulfide.

example of dolomite + magnesite in coarse-grained protogranular UZ peridotites. The interstitial dolomite grains are partly associated with magnesite (Fig. 5e, f). This sample also bears a vein of amphibole aggregates containing a 3-mm-large dolomite crystal. Fine veinlets consisting of dolomite associated with magnetite ± calcite ± (secondary?) serpentine(/chlorite?) crosscutting the pre-existing serpentine mesh texture were also rarely observed in one coarse-grained protogranular sample.

Calcite-brucite intergrowths

In the UZ peridotites, acicular calcite and brucite are finely intergrown (μm-scale; Figs. 8, 9, 10) and are found mostly in serpentinized fine-grained garnet-bearing samples, but are also observed in fine- and medium-grained garnet-free samples (Table 2). The texture of these calcite-brucite intergrowths indicates that they are pseudomorphs after dolomite and the conditions of dolomite retrogression will be discussed in chapter "Dedolomitization in Ulten Zone peridotites". Under the optical microscope, the different phases of the intergrowths are not distinguishable nor is the acicular shape visible (Fig. 9a, b). The intergrowths are noticeable as gray-black patches in both bright field view and cross-polarized view (Fig. 9a, b). The different phases of which the intergrowths are composed are distinguishable only with electron microscopy (Fig. 9c). The calcite-brucite intergrowths appear as grains with frayed grain boundaries and are commonly located within serpentinized parts of the peridotites, often contoured by Fe-oxide (magnetite; Fig. 9a-d), and in the peridotite matrix crosscut by serpentine veins (Fig. 9e). A textural relation to calcite veinlets within the serpentine phases is observed in some samples (Fig. 9d, f). In order to verify the mineralogical composition of these intergrowths, the relative abundance of elements (Ca, C, Mg, O, Fe) of selected areas of intergrowths was qualitatively measured. The relative element contents of all phases occurring in one intergrowth (sample WG1; Fig. 10) are shown as "false-color" element maps (Fig. 10b-f). The light gray part in the back-scattered-electron image (Fig. 10a) is clearly richer in Ca and C and poorer in Mg, O and Fe than the black part in the electron image. The key point regarding the element maps is that the black part is C-free, as the small C-content visible in the C-element map presumably derives from the carbon coating of the thin section. Comparison of the element abundances in the intergrowths confirmed the presence of brucite, a magnesium hydroxide ($Mg(OH)_2$). In the electron image (Fig. 10a), a darker gray phase occurring as patches between calcite and brucite is clearly visible and was identified as dolomite. According to this observation, in some samples some calcite-brucite intergrowths contain relics of dolomite (dolomite patches and/or dolomitic rims; Fig. 9f) indicating that dolomite was only partly replaced by calcite-brucite intergrowths.

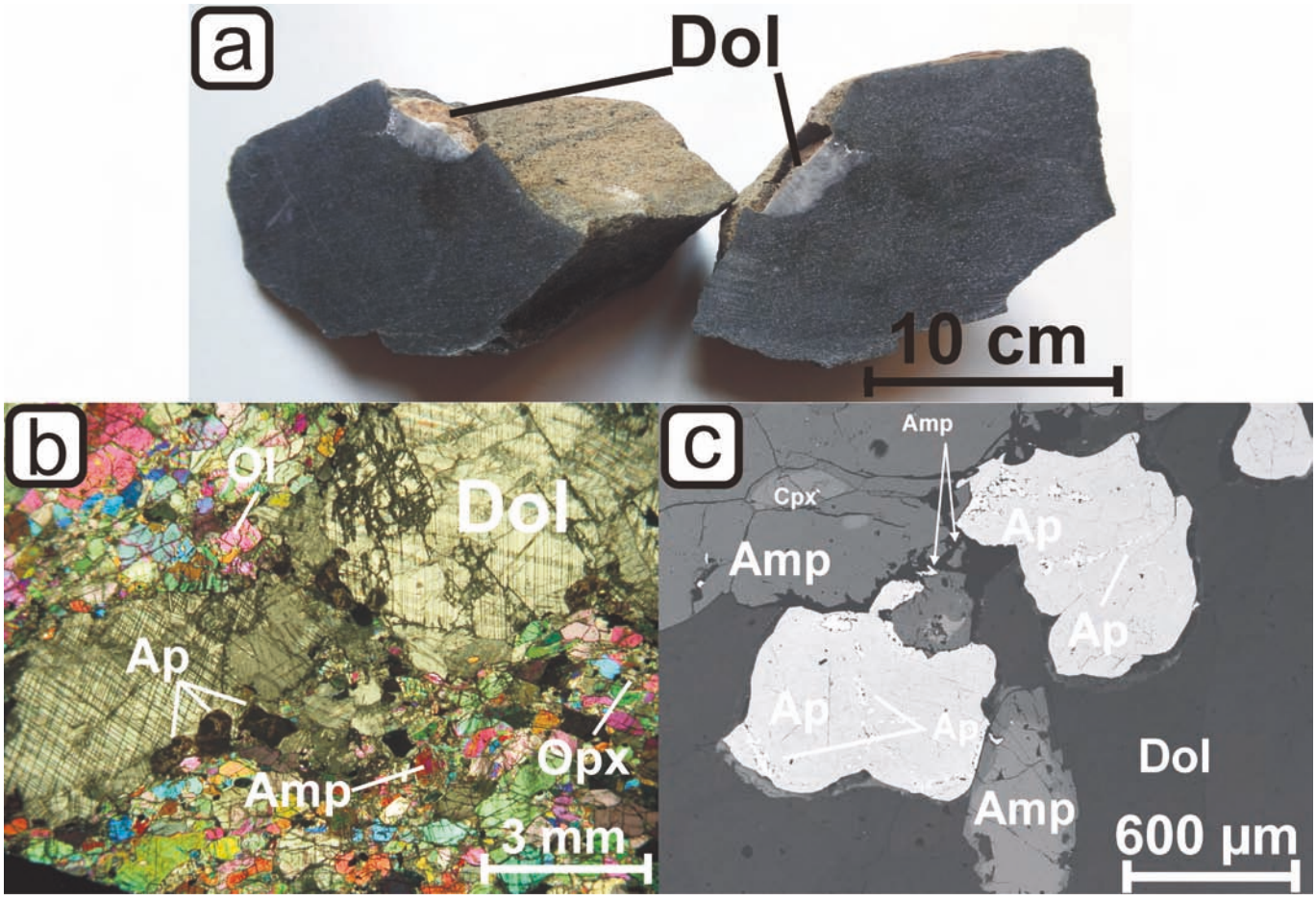

Fig. 6 - (a) Photograph of the hand specimen of sample VM25P11 with a lenticular polycrystalline aggregate of dolomite (~ 5 cm length); (b) polarized transmitted light photograph of a part of the polycrystalline aggregate of dolomite (thick section ~ 100 µm); (c) back-scattered electron image of the contact between the dolomite polycrystalline aggregate and matrix apatite and amphibole. Mineral abbreviations after Whitney and Evans (2010).

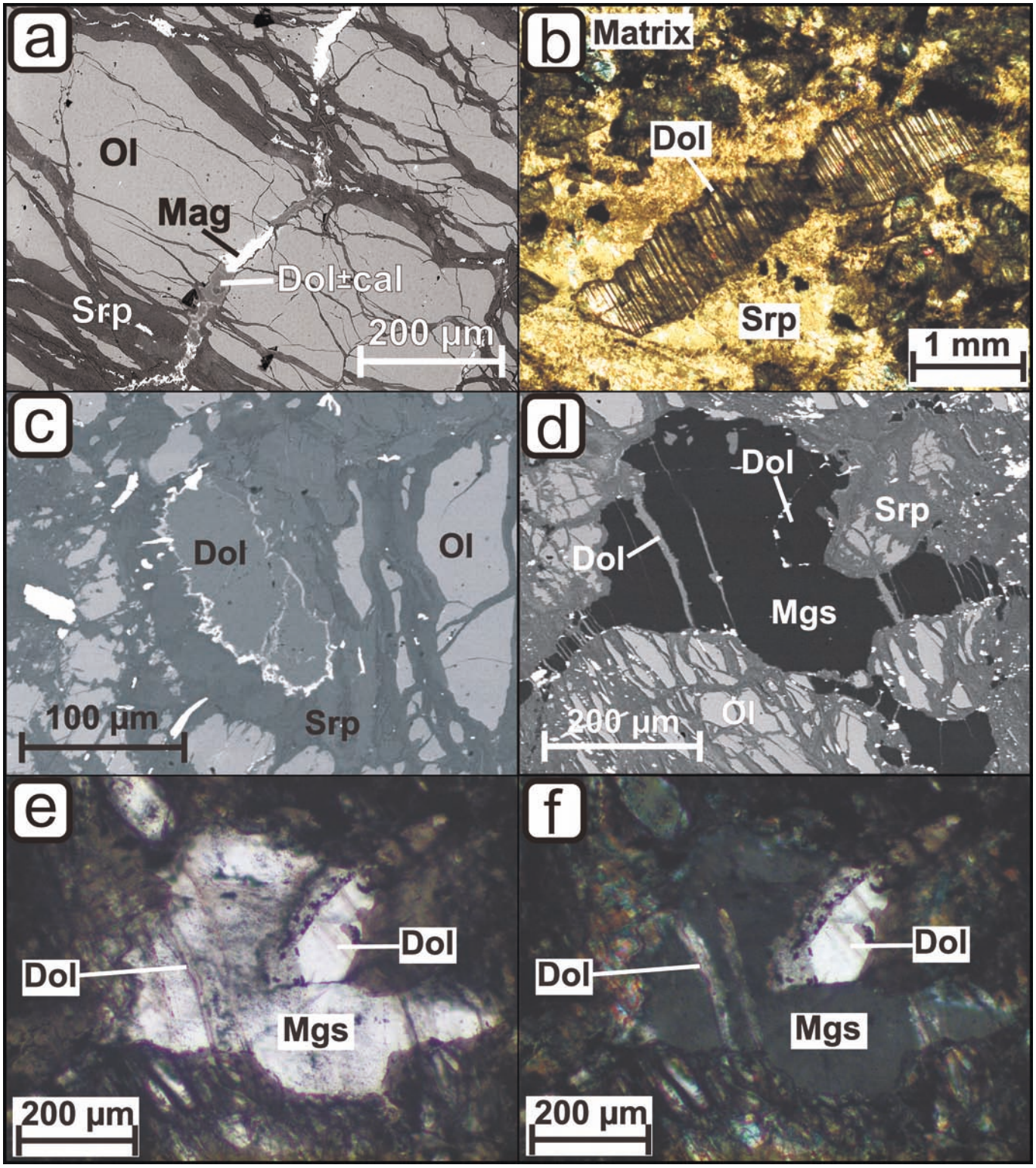

Fig. 7 - (a) Back-scattered electron (BSE) image of fine veinlets consisting of dolomite ± magnetite ± calcite ± serpentine crosscutting the pre-existing serpentine mesh texture in serpentinized fine-grained garnet-amphibole peridotites (WG1); (b) transmitted light photomicrograph of a distinct secondary serpentine vein (~ 3 mm thickness) containing discrete dolomite grains with frayed grain boundaries in a serpentinized fine-grained peridotite (MR141B, thick section ~ 100 μm); (c) back-scattered electron images of a dolomite grain with frayed grain boundary and associated with magnetite, located within the serpentine mesh texture of a serpentinized fine-grained garnet-amphibole peridotite (WG1); (d-f) back-scattered electron image (d), transmitted light photograph (e) and polarized transmitted light photograph (f) of a euhedral dolomite crystal (~ 150 μm length) associated with a magnesite aggregate located in the serpentine mesh texture of a serpentinized, highly mylonitic peridotite (SBB2F, thick section ~ 100 μm). The magnesite aggregate is interspersed with fine dolomite veinlets ("gray" in the BSE image), which are of different origin than the dolomite crystal ("black" in the BSE image). Mineral abbreviations after Whitney and Evans (2010).

Occasionally, distinct euhedral calcite-brucite intergrowths occur as inclusions in spinel, also in spinel which is itself enclosed in garnet, and as part of multi-phase solid inclusions (Fig. 8c). These inclusions are composed of calcite-brucite intergrowths + apatite ± serpentine ± sulfide ± ilmenite (Fig. 8c). The contact zones between spinel and garnet commonly consist of kelyphite. Also, grains of calcite-brucite intergrowths that are partly euhedral occur as inclusions in garnet (Fig. 8d),

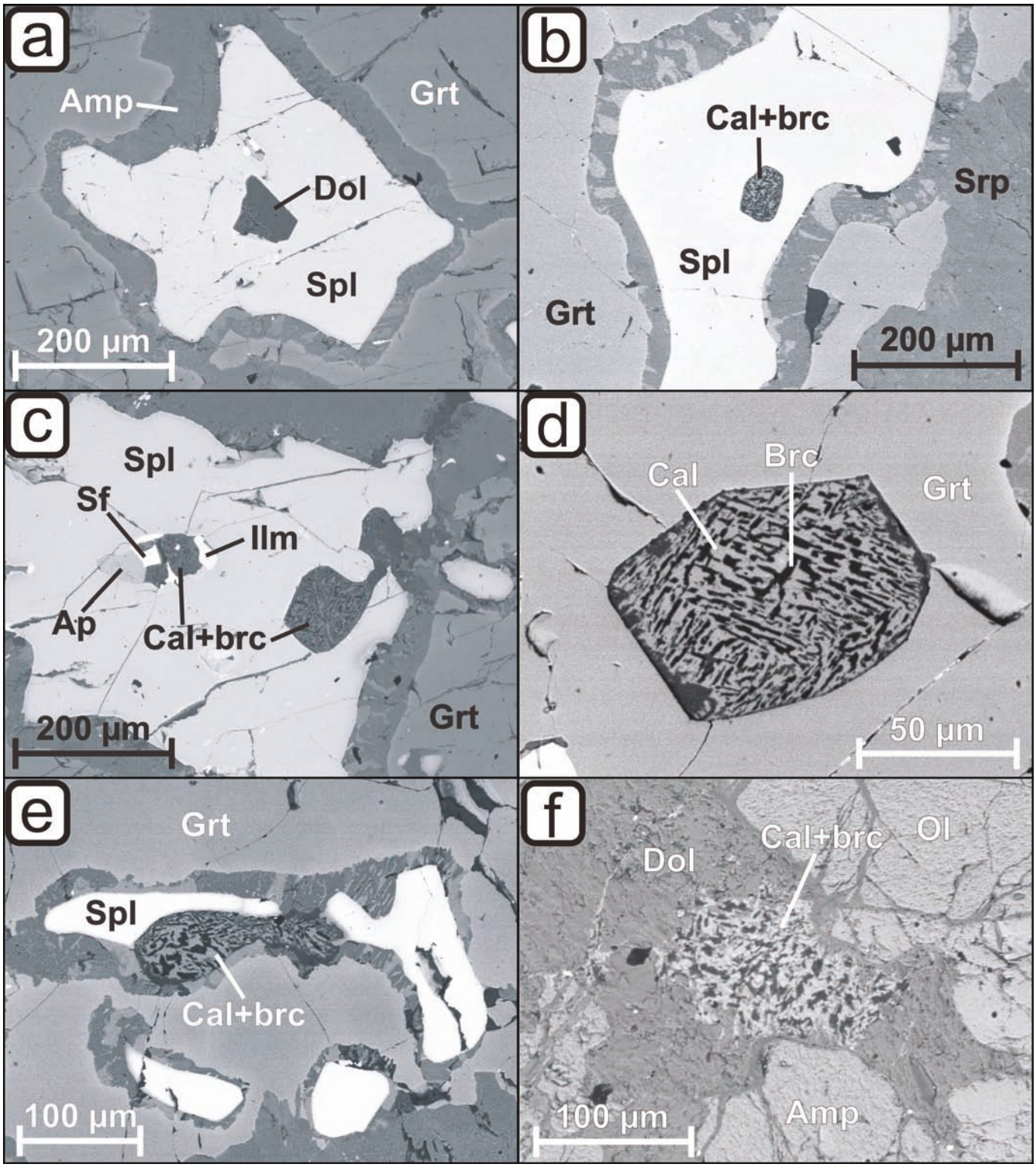

Fig. 8 - Back-scattered electron images of (a) an inclusion of euhedral dolomite in spinel surrounded by garnet in serpentinized fine-grained garnet-amphibole peridotite KL2.4-2b; (b) inclusion of calcite-brucite intergrowth in spinel surrounded by garnet in serpentinized fine-grained garnet-amphibole peridotite WG7; (c) calcite-brucite intergrowths as part of multi-phase solid inclusions in spinel in serpentinized fine-grained garnet-amphibole peridotite KL2.4-2b; (d, e) partly euhedral grains of calcite-brucite intergrowths as inclusion in garnet in serpentinized fine-grained garnet-amphibole peridotite (KBA8), (e) occasionally related to spinel hosted in garnet (WG7); (f) patch of calcite-brucite intergrowth with frayed grain boundary situated within a vein of associated anhedral dolomite and amphibole (KL1.6). Mineral abbreviations after Whitney and Evans (2010), sf- sulfide.

occasionally touching spinel (Fig. 8e) and/or related to serpentine. Finally, calcite + serpentine intergrowths as part of a multi-phase solid inclusion in spinel and in garnet related to a serpentine vein were observed. Patches of calcite-brucite intergrowths occur also situated within a vein of anhedral dolomite referred to earlier (chapter "Dolomite", Fig. 5c, d). Also, veins consisting of calcite + brucite occur in serpentine veins and are there interlaced with serpentine and magnetite (Fig. 11a, b).

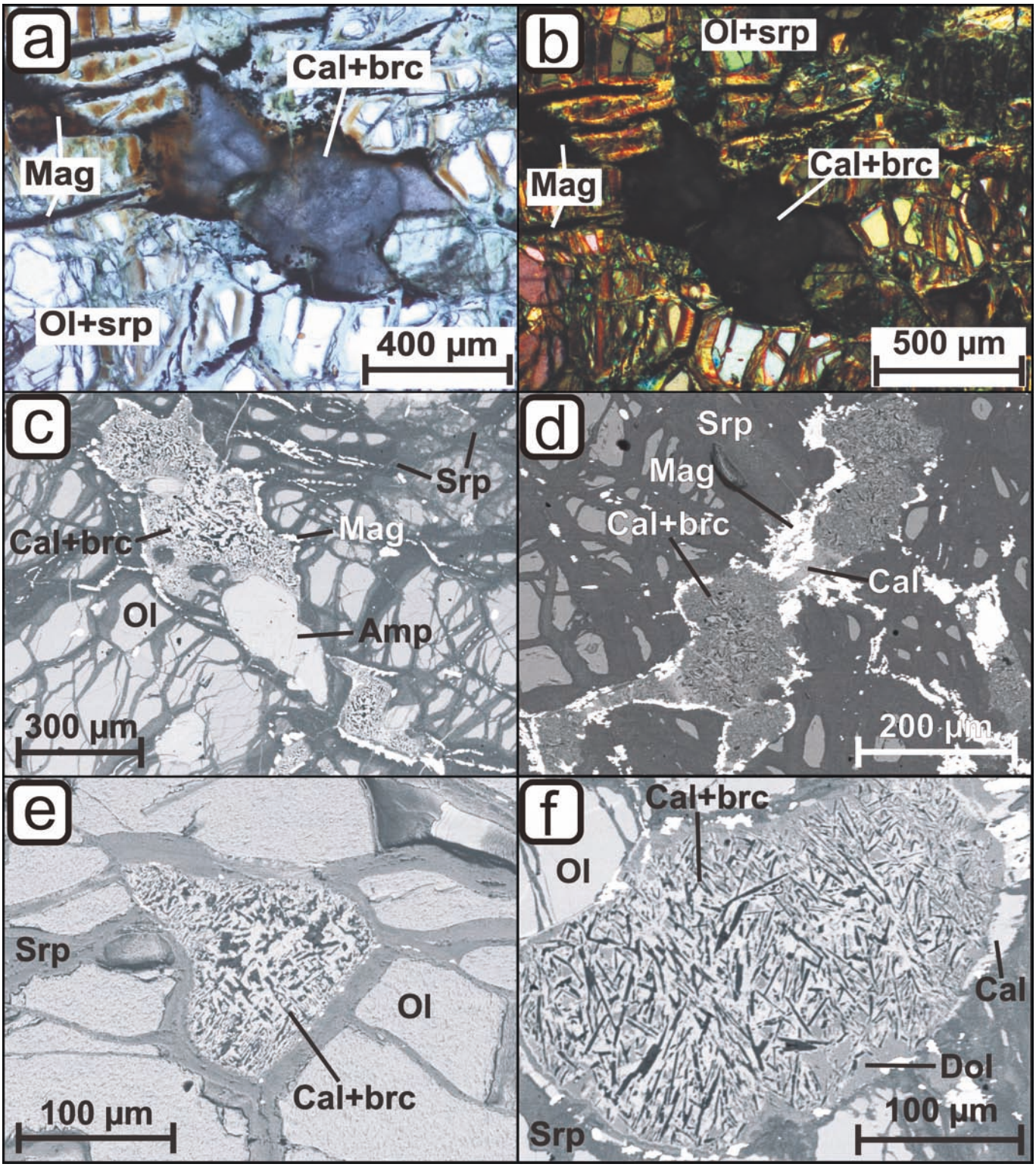

Fig. 9 - (a) Transmitted light photograph, (b) polarized transmitted light photograph and (c) back-scattered electron image of an intergrowth of acicular calcite and brucite located within the serpentine mesh texture in serpentinized fine-grained garnet-amphibole peridotite PL1.6, associated with amphibole and magnetite (thick section ~ 100 μm); (d-f) back-scattered electron images of calcite-brucite intergrowths in serpentinized fine-grained garnet-amphibole peridotites, (d) contoured by magnetite and associated with calcite patches, located within serpentinized parts (SB2-2), (e) located in the peridotite matrix crosscut by serpentine veins (KL1.3c), (f) with interspersed dolomite patches, located within the serpentine mesh texture, associated with magnetite, contoured by calcite veinlets (WG1). Mineral abbreviations after Whitney and Evans (2010).

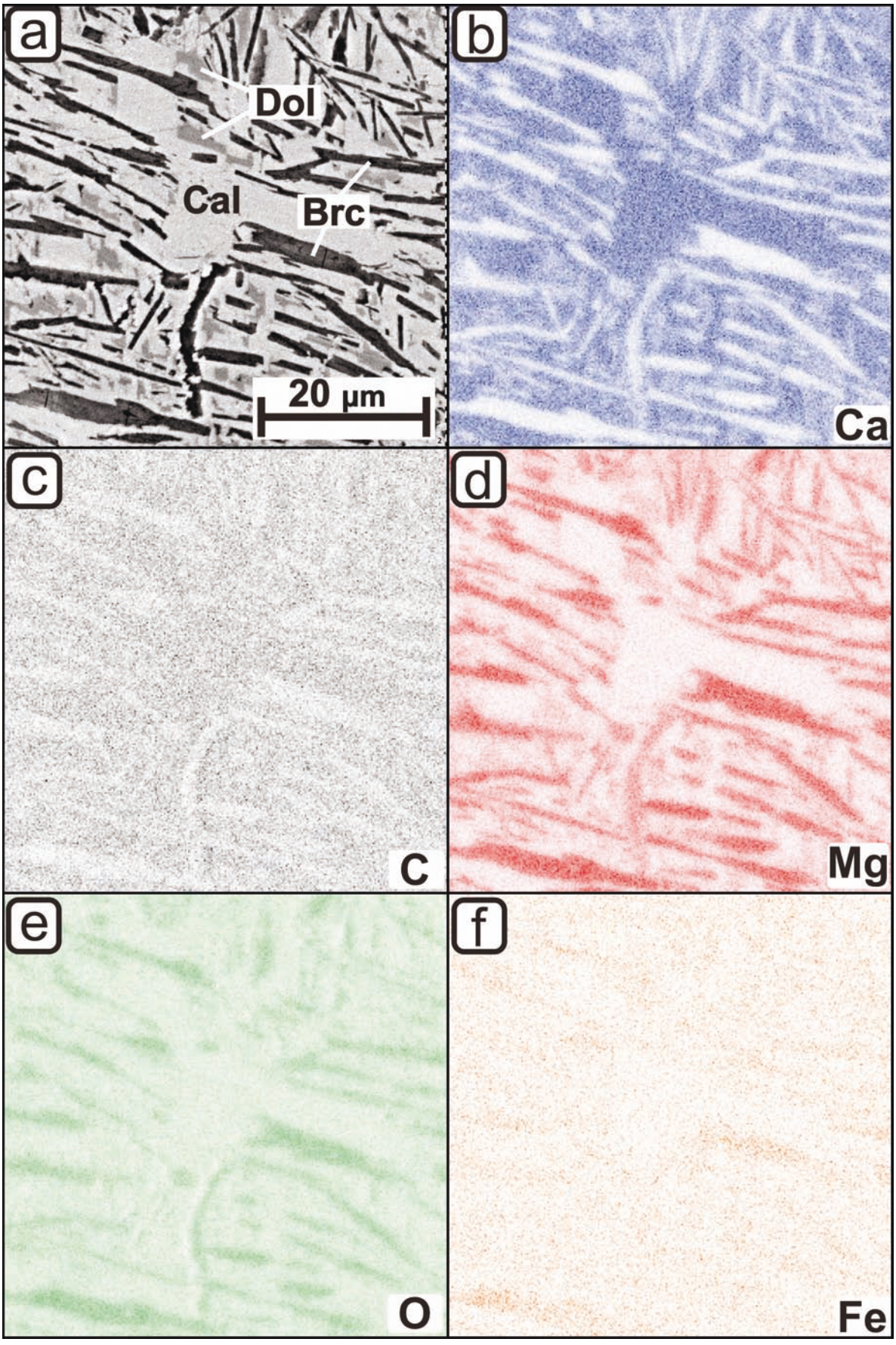

Fig. 10 - (a) Back-scattered electron image of an intergrowth of calcite (light gray phase) and acicular brucite (black phase) with interspersed dolomite patches (dark gray phase); (b-f) "false-color" element maps of the calcite-brucite intergrowths showing the distribution of (b) calcium, (c) carbon, (d) magnesium, (e) oxygen and (f) iron between the mineral phases. In the element maps (b-f) dark areas denote high element abundances and light areas denote low element abundances. Mineral abbreviations after Whitney and Evans (2010).

With one exception of a serpentinized coarse-grained sample, neither coarse-grained garnet-free nor garnet-bearing samples contain calcite-brucite intergrowths. This is in agreement with the lack of precursor dolomite in these samples.

Calcite veinlets

Fine veinlets (a few μm thick) and patches consisting of calcite occur in both fine- and medium-grained garnet-free peridotites and in garnet-bearing peridotites, as well as in coarse-grained garnet-free peridotites (Table 2; Fig. 11c, d). These calcite veinlets and patches are often situated within the serpentinized mesh texture in both fine-grained and coarse-grained peridotites where they are often associated with magnetite (Fig. 11c). In this textural context, calcite veinlets are occasionally spatially closely related to the calcite-brucite intergrowths, often contouring the calcite-brucite grain boundaries (fine-grained garnet-bearing peridotites; Fig. 9f). As mentioned in chapter "Dolomite", veinlets of calcite + dolomite + magnetite occur occasionally in serpentinized fine-grained garnet-bearing samples (Fig. 7a). Calcite veinlets also crosscut mineral grains such as amphibole, clinopyroxene, garnet and spinel (Fig. 11d).

Magnesite

In the studied sample set, magnesite occurs as anhedral grains in textural equilibrium with dolomite, as veins on a μm-to-mm scale (Table 2), commonly situated within serpentine veins or the serpentine mesh texture in both coarse-grained and fine-grained garnet-free peridotites. In one coarse-grained protogranular sample, interstitial anhedral dolomite and magnesite are in textural equilibrium (Fig. 5e, f) and are spatially closely related to a ~ 500 μm thick distinct magnesite vein (not shown) with frayed boundaries. This vein crosscuts the ultramafic mineral assemblage perpendicularly to the rock fabric. This is true also for a ~ 2 mm thick magnesite vein in a fine-grained garnet-free sample (Fig. 11e). Another fine-grained garnet-free sample contains an anhedral magnesite aggregate in textural equilibrium with a euhedral dolomite crystal, situated in the serpentine mesh texture (Fig. 7d-f). In this sample, magnesite also occurs as irregularly aligned grains embedded in a fine serpentine vein with sharp boundaries crosscutting the ultramafic mineral assemblage. A similar vein consisting of serpentine + magnesite occurs also in another coarse-grained protogranular peridotite (Fig. 11f).

DISCUSSION

The occurrences of different carbonates in the mantle wedge-derived ultramafic rocks from the UZ will be discussed in the following in the context of the regional tectonometamorphic evolution. The various mineralogical and microstructural peridotite types (Table 2) record different petrologic processes in the Ulten Zone and can be linked to particular carbonate minerals, associations and textures. Thus, this relationship may reflect different stages of carbonate formation and carbonate breakdown/replacement (stages 1-6, Figs. 12, 13) accompanying the evolution of the UZ tectonic unit (Fig. 12b) during continental collision.

Carbonate inclusions in primary spinel: indicator for the mobilization of carbonated silicate melt in the hot mantle wedge

The dolomite inclusions, the calcite-brucite intergrowths after former dolomite (see chapter "Dedolomitization in Ulten Zone peridotites") and the carbonate-bearing multi-phase solid inclusions (calcite-brucite + apatite ± ilmenite ± sulfide ± serpentine) entrapped in garnet-hosted coarse spinel (Fig. 8a-c) indicate early carbonate formation in the UZ mantle wedge in the high-temperature spinel stage (stage 1, Figs. 12, 13). Recent studies report the occurrence of multi-phase solid inclusions containing a carbon component in spinel in both orogenic peridotites (Zaccarini et al., 2004; Carswell and Van Roermund, 2005; Naemura et al., 2009) and peridotite xenoliths (Timina et al., 2012). For the first case, two hypotheses of carbon introduction into the mantle have been postulated: (1) The origin of such multi-phase inclusions in high-T Cr-spinel has been attributed to the reaction of protolith-peridotite with alkaline-carbonatite fluids formed from an original carbonatitic melt and a hydrous fluid, presumably generated during the emplacement of a mantle plume and mantle uplifting (Zaccarini et al., 2004). (2) Carbonate-bearing multi-phase inclusions (together with microdiamonds) originate from a supercritical COH-fluid that was generated during UHP-prograde dehydration and decarbonation reactions in a subducting continental slab (Carswell and Van Roermund, 2005). For peridotite xenoliths, it has been assumed that carbonate-water-chloride-rich fluids caused metasomatism accompanied by the formation of carbon-bearing solid inclusions in spinel (Timina et al., 2012). Supercritical fluids (which can vary from pure H_2O to hydrous melt) are restricted to ultrahigh-pressure conditions (e.g., Manning, 2004) in subduction zones and may not play a role during continental subduction. Oceanic subduction prior to continental subduction might have been associated with carbonate dissolution and silico-carbonatite formation in the supra-subduction mantle wedge as modelled by Tumiati et al. (2013). Evidence for carbonate dissolution in both oceanic and continental ultra-high pressure rocks have been reported recently (e.g., Frezzotti et al., 2011; Ferrando et al., 2017) and hydrous carbonatitic liquids were recently shown to form at temperatures down to 870°C to 900°C (Poli, 2015). Such liquids may have been liberated from a former oceanic slab and migrated upward into the hot portion of the wedge. In this case, dolomite and/or dedolomitization products would be expected also in spinel peridotites that never equilibrated in the garnet-stability field. However, matrix dolomite and/or calcite-brucite intergrowths have not been observed in coarse-grained spinel peridotites or in the few fine-grained (post-)garnet-free peridotites available for study. On the other hand, Scambelluri et al. (2006) suggested that primary spinel lherzolites in the mantle wedge were infiltrated by subduction-related mafic melts which derived from deeper magma sources and carried recycled crustal components. We infer that these subduction-related mafic melts carried a carbon component responsible for the formation of carbonate in the multi-phase solid inclusions in spinel. The mineral assemblage in the multi-phase solid inclusions is not indicative of the pressure and temperature conditions at the time of entrapment of the melts. This assemblage precipitates during the subsequent evolution of the rock and may be, therefore, used to constrain the chemical composition of

the melt (Frezzotti and Ferrando, 2015). Stage 1 in Fig. 12 may, however, depict the conditions for the entrapment of the carbon-bearing melts in spinel. Considering their high-temperature mantle wedge origin, dolomite formation in the spinel peridotites likely predated entrainment in the subducting slab and associated metasomatic reactions.

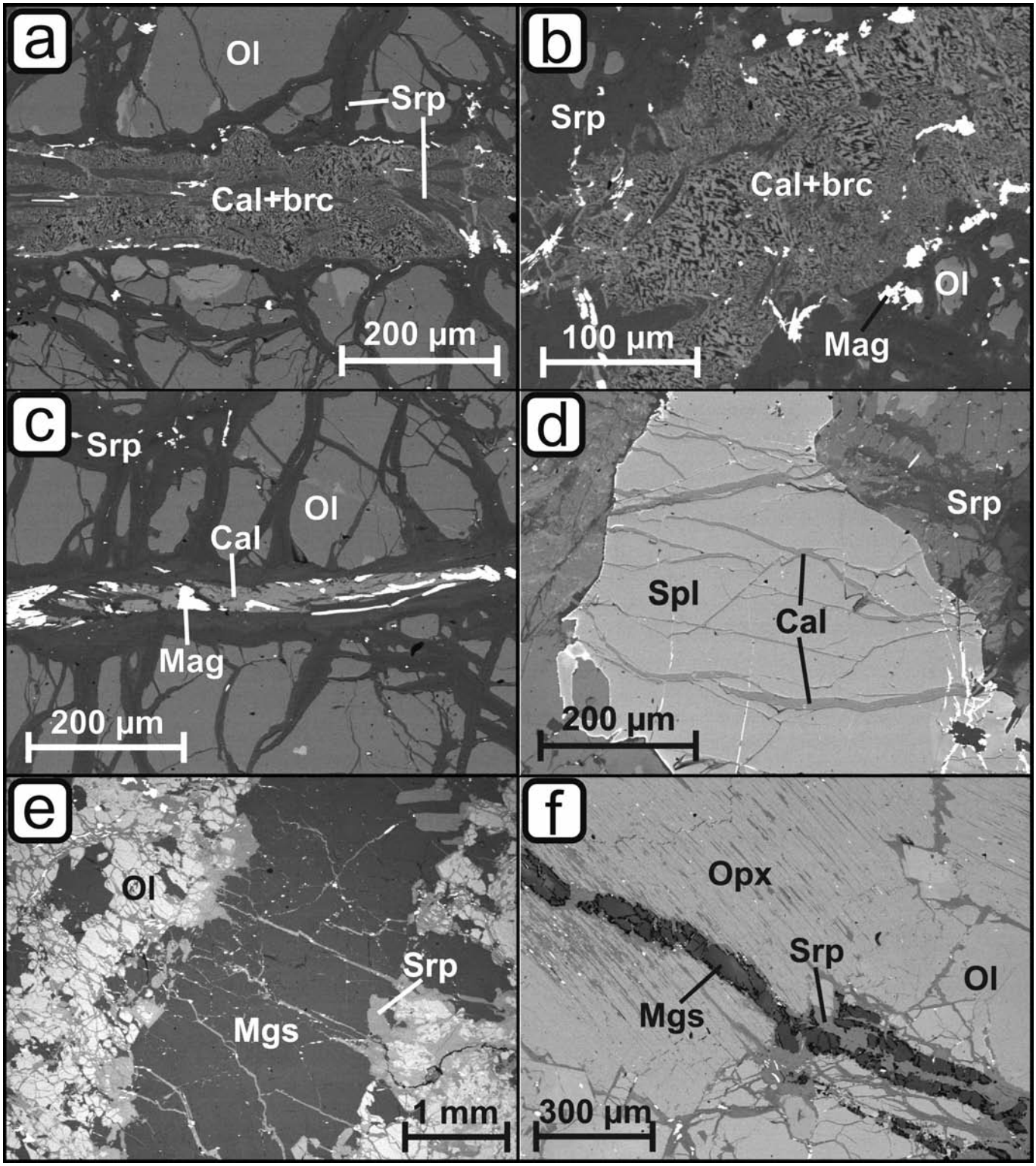

Fig. 11 - Back-scattered electron images of (a, b) a vein (~ 150 μm thickness) consisting of calcite-brucite intergrowths situated within a serpentine vein in serpentinized medium-grained peridotite KoDb2. The intergrown acicular calcite and brucite are interlaced with serpentine and magnetite; (c) calcite veinlet related to magnetite situated in the serpentine mesh texture of serpentinized medium-grained peridotite KoDb2; (d) calcite veinlets in spinel in serpentinized medium-grained peridotite KoDb2; (e) distinct magnesite vein with frayed boundaries in the mineral assemblage of serpentinized fine-grained garnet-free sample KoD9; (f) magnesite grains embedded in distinct serpentine vein with sharp boundary occurring within the ultramafic mineral assemblage of coarse-grained protogranular peridotite KoD4 as well as intersecting orthopyroxene and olivine in this sample. Mineral abbreviations after Whitney and Evans (2010).

Dolomite formation from crust-derived aqueous fluids at high pressures

In previous studies based on porphyroclastic and fine-grained garnet peridotites it has been consistently suggested that matrix dolomite and the coexisting hydrous phases (pargasitic amphibole ± phlogopite) plus apatite are of metasomatic origin and crystallized in equilibrium with garnet from aqueous COH-fluids in the garnet-stability field (Obata and Morten, 1987; Godard et al., 1996; Rampone and Morten, 2001; Tumiati et al., 2003; Marocchi et al., 2009; Sapienza et al., 2009). Such fluids have been interpreted to derive from a hydrous silicate melt released from the continental slab during migmatization of the host gneiss (Rampone and Morten, 2001; Tumiati et al., 2003; Sapienza et al., 2009) ca. 330 Ma ago (Tumiati et al., 2003). The low dolomite/amphibole proportion in the peridotites has been interpreted to reflect a low CO_2/H_2O ratio of the metasomatic fluid (Rampone and Morten, 2001).

In the present study, the fine-grained garnet-amphibole peridotites contain dolomite disseminated within the peridotite matrix (Fig. 3), dolomite in a multi-phase solid inclusion in garnet (Fig. 4e) as well as calcite-brucite intergrowths, which are interpreted to be dedolomitization products (chapter "Dedolomitization in Ulten Zone peridotites"), as inclusions in garnet (Fig. 8d, e). The occurrences of dolomite in the multi-phase solid inclusion and of inclusions of calcite-brucite intergrowths in garnet lends strong support to the inference that the formation of dolomite occurred during garnet formation (stage 2, Figs. 12, 13). Dolomite inclusions in matrix apatite and amphibole (Fig. 4a, b) in these garnet-amphibole peridotites and the occasional close spatial relation between dolomite and these phases in the peridotite matrix (Fig. 3) further support the assumption that they co-precipitated from a phosphorus-bearing COH-fluid. The rare observations of dolomite inclusions in matrix olivine (Fig. 4c, f) in fine-grained garnet-amphibole peridotites indicate that the interaction of wedge peridotite with crust-derived fluids might have accompanied the formation of garnet + olivine at the expense of spinel + orthopyroxene + clinopyroxene (e.g., Jenkins and Newton, 1979; Obata and Morten, 1987; Klemme and O'Neil, 2000). Overall, based on P-T estimates for anhydrous peridotites (Nimis and Morten, 2000), Sapienza et al. (2009) suggested high-pressure dolomite formation (~ 2.5 GPa and 850-900°C, < 100 km depth) and an additional dolomite formation episode at low-pressure retrograde metamorphic conditions (1.5-1.8 GPa and < 850°C, shallow depths) in the UZ peridotites. The latter is consistent with the absence of primary discrete magnesite in the samples studied here, in accord with previous observations in UZ peridotites (Malaspina and Tumiati, 2012) and experimental results (magnesite stability > 1.9 GPa at 900°C, Tumiati et al., 2013). Additionally, based on experimentally determined garnet stability in COH-bearing peridotites (Tumiati et al., 2013), it can be inferred that T ≥ 900°C at 1.9 GPa is required for dolomite formation when garnet is stable (stage 2, Figs. 12, 13). Nevertheless, the association of dolomite, chlorite and dissakisite in the multi-phase solid inclusion in garnet (Fig. 4e) may have crystallized at lower temperatures from a fluid inclusion entrapped in garnet. Tumiati et al. (2005; 2007) suggested that the mineral dissakisite-(La) ($CaLaAl_2MgSi_3O_{12}(OH)$), which is enriched in large ion lithophile elements (LILE), crystallized from crust-derived aqueous fluids at P ≤ 2.7 GPa and T ≤ 850°C. In this case the mineral association of the multi-phase solid inclusion would reflect the chemical composition of the carbon-bearing LILE-rich aqueous fluid which infiltrated the peridotites during the garnet-forming stage. The occurrence of dolomite + apatite as inclusion in zircon may be, as well, related to this stage. However, future geochronological and chemical analyses of the zircon will address the formation conditions of zircon in the UZ peridotites and the occurrence of dolomite inclusions in zircon.

In contrast to the fine-grained garnet-bearing peridotites, coarse garnet- and spinel peridotites commonly contain amphibole but generally neither apatite nor dolomite nor calcite-brucite intergrowths (except sample MOL1.5; Table 2). Tumiati et al. (2003) report that peridotite portions in the mantle wedge can escape hydration while other portions undergo infiltration of aqueous fluids and partial dolomite (re)crystallization. Accordingly, the absence of dolomite, calcite-brucite intergrowths as well as apatite in both coarse-grained spinel- and garnet peridotites suggests their preservation as lenses within the fine-grained host peridotites. This is in agreement with our field observation of the occurrence of coarse-grained peridotite as relics embedded within deformed fine-grained peridotite (Fig. 2). In one locality (Samerbergalm), coarse-grained garnet-peridotites that are free of carbonate and apatite are spatially closely related, at meter scale, to the dolomite-bearing fine-grained garnet-amphibole peridotites. This structural occurrence might be attributed to the entrapment of fine-grained garnet-peridotites by the continental slab and attendant shearing, deformation and hydration/carbonation while the coarse peridotite was embedded and shielded from these processes.

Local formation of dolomite + magnesite from continental crust-derived aqueous fluids

Stability of magnesite + dolomite outside garnet stability can be achieved in a small P-T window (at ~ 1.8-2.0 GPa and at 850-900°C; stage 3, Fig. 12) in the pressure and temperature range covered by the experiments by Tumiati et al. (2013). The only garnet-free sample containing associated anhedral magnesite and dolomite is a coarse-grained non-serpentinized peridotite (MOL1.5; Fig. 5e, f) that probably never equilibrated in the garnet-stability field. The coexistence of interstitial anhedral dolomite and a magnesite vein in this sample indicates local injection of a crust-derived C-rich aqueous fluid with high CO_2/H_2O ratio. The absence of antigorite and chlorite in this sample shows that this peridotite-fluid interaction occurred indeed in the P-T window between the chlorite-out and garnet-in curves (stage 3, Fig. 12). Interestingly, the location of stage 3 (magnesite + dolomite in garnet-free peridotite) in the P-T diagram (Fig. 12) overlaps the P-T estimates for equilibration of dolomite-bearing hydrous garnet-amphibole peridotite at ~ 1.8-2.2 GPa and > 800°C from Braga and Sapienza (2007). These P-T conditions were calculated considering a COH-fluid with X_{CO2} = 0.1 (Braga and Sapienza, 2007) and are in agreement with P-T estimates of 1.96 GPa and minimum temperature of 841°C by Malaspina and Tumiati (2012) for a dolomite + orthopyroxene inclusion in garnet. The discrepancy between these P-T estimates and those of Tumiati et al. (2013) might be explained by different X_{CO2} and/or other conditions for the calculations. Considering the experimentally determined phase relations by Tumiati et al. (2013), the temperature estimates for dolomite formation in garnet-amphibole peridotite by Braga and Sapienza (2007) and Malaspina and Tumiati (2012) are underestimated.

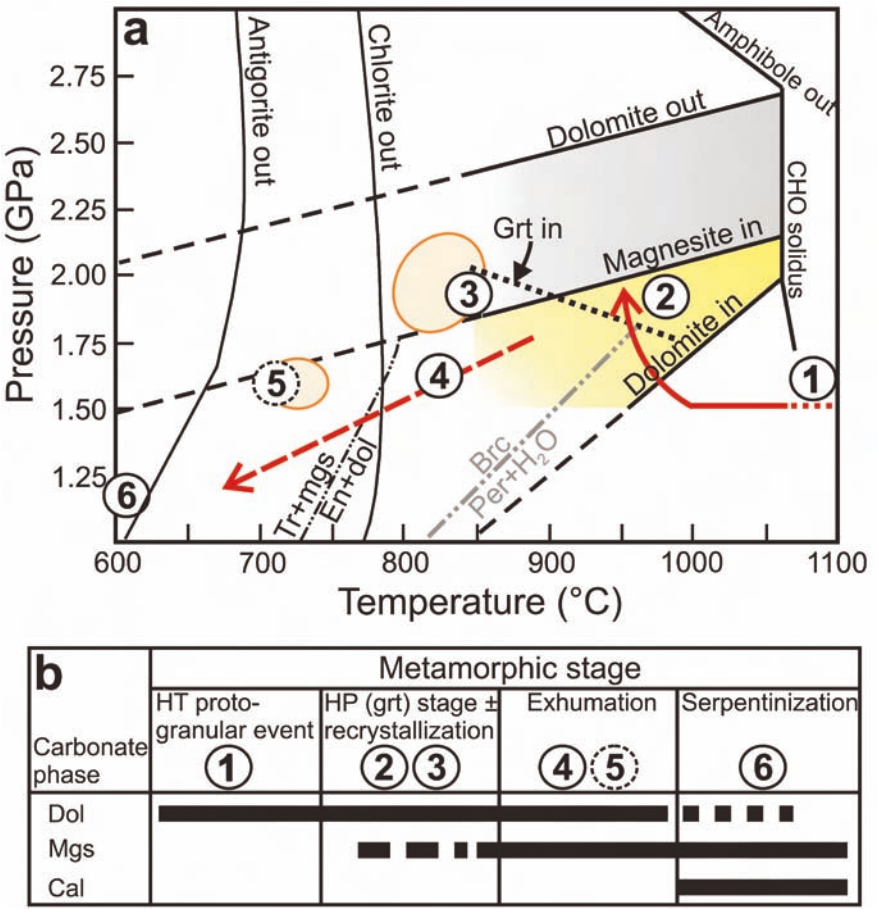

Fig. 12. (a) Pressure-temperature diagram with stages of carbonate formation in the tectonometamorphic evolution of the Ulten Zone peridotites (1-6). The circle in stage 5 is dashed because the position of this stage in the diagram is only a possibility and may be shifted to lower pressures and temperatures in the antigorite stability field. Stability of dolomite (yellow shaded field) and dolomite + magnesite (gray shaded field) 1.5 GPa and 850°C (full lines) in the peridotite-COH system is taken from Tumiati et al. (2013) and extrapolated to lower pressures and temperatures (dashed lines). Dolomite-in, magnesite-in and dolomite-out curves from Tumiati et al. (2013) refer to carbonate formation from COH-fluids. Univariant reaction tremolite (tr) + magnesite (mgs) = enstatite (en) + dolomite (dol) taken from Malaspina and Tumiati (2012) for X_{CO2} = 0.5. Garnet-in curve based on experimental results of Tumiati et al. (2013). P-T curve for the brucite (brc) = periclase (per) + water (H_2O) equilibrium from Schramke et al. (1982). Antigorite-out curve and chlorite-out curve from Fumagalli and Poli (2005). Ovals overlapping with stage 3 and stage 5 mark P-T estimates for dolomite-bearing garnet-amphibole and chlorite-amphibole assemblages, respectively, from Braga and Sapienza (2007). Dotted red arrow marks cooling and pressure decrease from magmatic conditions due to corner flow, full red arrow marks isobaric cooling and subduction path of the Ulten Zone peridotites, dashed red arrow marks direction of exhumation path. (b) Table showing the stages of carbonate formation (stages 1 to 6) and carbonate stability linked to metamorphic stages of the Ulten Zone peridotites. HT: high temperature, HP: high pressure. Mineral abbreviations after Whitney and Evans (2010).

Dolomite in retrogression textures and dolomite veins: indicators for low-pressure carbonation?

The occurrence of interstitial band-like dolomite and distinct dolomite veins (Fig. 5b-d) related to amphibole in weakly serpentinized fine-grained peridotites leads to the assumption that at a certain stage on the exhumation path (stage 4, Fig. 12) C-rich fluids prompted dolomite precipitation. This is in agreement with the occurrence of anhedral dolomite grains in amphibole-rich domains that were interpreted to derive from a COH-fluid during low-pressure retrograde conditions (Sapienza et al., 2009). Considering the low abundance of these dolomite veins and their limited extent, such fluids probably occurred only locally (similar to the carbonate occurrence in sample MOL1.5, discussed in chapter "Local formation of dolomite + magnesite ….".). The veins consisting of calcite-brucite intergrowths observed in two serpentinized fine-grained samples (Fig. 11a, b) crosscut the peridotite embedded in the serpentine mesh texture. This may indicate that the local formation of dolomite veins from a C-rich aqueous fluid occurred at a time after high-pressure dolomite formation (stage 2) and prior to low-temperature serpentinization during exhumation. The occurrence of dolomitic veinlets crosscutting the serpentine mesh texture (Fig. 7a) and dolomite grains within a distinct serpentine vein (sample MR141B, Fig. 7b) show that additional pulses of probably C-rich, aqueous fluids percolated the peridotites syn- and/or post-serpentinization during exhumation. It has been suggested that during exhumation a dolomite-magnesiohornblende-bearing garnet-free assemblage develops at ~ 1.8 GPa and ≥ 790°C (Malaspina and Tumiati, 2012). At these retrograde metamorphic conditions, dolomite occurs as part of a kelyphitic assemblage (orthopyroxene + magnesiohornblende + spinel + minor dolomite) around garnet, while larger dolomite neoblasts, orthopyroxene, magnesiohornblende and olivine constitute the stable matrix assemblage (Malaspina and Tumiati, 2012). These observations might be in agreement with the dolomite in garnet pseudomorphs (Fig. 5a) and kelyphitic coronas in some fine-grained peridotites that once equilibrated in the garnet-stability field. However, the question arises if low-pressure formation of dolomite + magnesiohornblende by crust-derived aqueous fluids (Sapienza et al., 2009) during exhumation overprinted or recrystallized a pre-existing dolomite-bearing assemblage, which originally formed at higher pressure conditions while garnet was stable. If dolomite neoblasts that are ascribed to crystallization at equilibrium with garnet (Sapienza et al., 2009) coexist with retrograde dolomite in kelyphites, low-pressure retrograde ingress of COH-fluids would form new dolomite but not destabilize the pre-existing matrix dolomite. Chemical analyses of dolomites and associated amphiboles will help distinguish between different stages of dolomite formation. In this context, it must be noted that it remains subject of debate whether the polycrystalline dolomite aggregate (Fig. 6) can be attributed to high-pressure dolomite formation during garnet stability (stage 2) or to low-pressure formation of vein-like dolomite (stage 4).

Formation of retrograde magnesite

In contrast to magnesite + dolomite in sample MOL1.5 (chapter "Local formation of dolomite + magnesite ….")

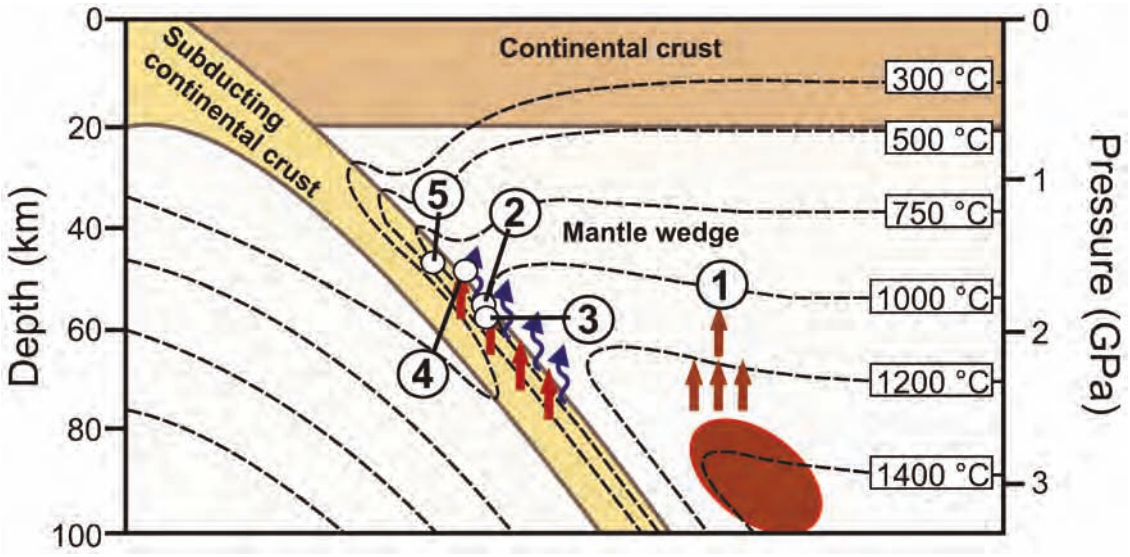

Fig. 13. Schematic illustration of continental subduction and a possible scenario of the Ulten Zone evolution with different stages of carbonate formation. Infiltration of carbonated silicate melts or COH-fluids (oval and arrows, stage 1) derived from an oceanic slab prompting dolomite formation during the high-temperature spinel stage. This is followed by isobaric cooling of peridotite as corner flow drags the mantle towards the cooler slab and infiltration of slab-derived aqueous COH-fluids (thin blue arrows), again leading to dolomite formation (stage 2). The COH-fluids are residual from reaction of slab-derived hydrous silicate melt (small red arrows in slab) with the mantle wedge (Rampone and Morten, 2001). During this event, at slightly higher pressure but lower temperature in the subduction mélange, these fluids lead to the formation of associated dolomite and magnesite in the peridotite (stage 3). Exhumation starting at ca. 330 Ma (Tumiati et al., 2003) was accompanied by several stages of carbonate formation in the Ulten Zone peridotites, i.e. formation of interstitial vein-associated dolomite, again from continental slab-derived aqueous fluids, at lower pressure and temperature (stage 4) and formation of retrograde magnesite (±dolomite) from C-rich aqueous fluids (stage 5).

the anhedral magnesite aggregate touching a euhedral dolomite crystal (Fig. 7d-f) in a garnet-free serpentinized fine-grained peridotite (sample SBB2F) is set in the serpentine mesh and presumably of different origin than the dolomite + magnesite in sample MOL1.5. The stability of magnesite + dolomite might be achieved at lower pressures and temperatures during retrograde metamorphic stages (Malaspina and Tumiati, 2012). These authors report the formation of magnesite coronas around dolomite attributed to the transition from magnesiohornblende-dolomite peridotite to chlorite-tremolite-magnesite peridotite with decreasing pressure and temperature in the UZ (Malaspina and Tumiati, 2012). Retrograde magnesite formation in this mineral assemblage is consistent with the P-T estimates of Braga and Sapienza (2007) of ~ 730°C at ~ 1.6 GPa (Malaspina and Tumiati, 2012) for X_{CO2} = 0.5 for garnet-free, carbonate-bearing peridotite. Stage 5 in Fig. 12 marks a possible location of retrograde magnesite formation as observed in sample SBB2F according to the P-T estimates of Braga and Sapienza (2007) and the univariant reaction tremolite + magnesite = enstatite + dolomite + H_2O + CO_2 modelled by Malaspina and Tumiati (2012), also considering X_{CO2} = 0.5. Interestingly, the P-T estimates of dolomite-bearing chlorite-amphibole peridotite of Braga and Sapienza (2007) plot in the magnesite-stability field estimated by Malaspina and Tumiati (2012). Those for the dolomite-bearing assemblage depend on the X_{CO2} in the fluid (Braga and Sapienza, 2007) and a lower X_{CO2} would shift magnesite stability to higher P-T conditions. This might explain the absence of magnesite in this assemblage and the discrepancy of the different P-T estimates. For the magnesite + dolomite-bearing sample SBB2F, pre-existing dolomite may have decomposed leading to the formation of magnesite. Alternatively, sample SBB2F never contained dolomite (as e.g., from stage 2, since further dolomite has not been observed in this sample). In this case, dolomite + magnesite might have formed from a COH-fluid at high X_{CO2}, which shifts the COH-fluid magnesite-in curve to lower pressures (Tumiati et al., 2013). The coexistence of magnesite + dolomite with serpentine in this sample may indicate that the carbonate phases were stable at even lower temperatures (< 730°C) in the antigorite stability field during exhumation. In this case, magnesite might coexist with antigorite at exhumation P-T conditions. Common stability of carbonate phases and serpentine might, thus, indicate elevated X_{CO2} (> 0.5?) in the metasomatizing fluid. Alternatively, they formed at higher temperatures and persisted metastably because fluid flow subsequently was insufficient to catalyze their breakdown. This might also apply to the magnesite vein in serpentinized sample KoD9 (Fig. 11e).

Dedolomitization in Ulten Zone peridotites

Intergrowths of calcite and the magnesium hydroxide brucite ($Mg(OH)_2$) in natural ultramafic rocks have been rarely observed to date. Berg (1986) first reported the presence of finely intergrown calcite and brucite in mantle-derived xenoliths in diamond-bearing volcanic kimberlite of the Kimberly pipe, South Africa. These calcite-brucite intergrowths were observed in coarse garnet lherzolite, porphyroclastic lherzolite and porphyroclastic wehrlite and were interpreted to reflect the breakdown products of dolomite (Berg, 1986). We here present a new observation

of calcite-brucite intergrowths as dedolomitization products in wedge-derived peridotite. This interpretation is supported by the occurrence of dolomite patches within the intergrown calcite and brucite (Fig. 9a), which may represent relict dolomite from incomplete dolomite breakdown. Also, located in the ultramafic matrix, the calcite-brucite intergrowths often inherit the grain shape of former discrete dolomite. Since the occurrence of calcite-brucite intergrowths is commonly associated with serpentinization, we suggest that the breakdown of dolomite in the UZ peridotites is linked to the reaction with serpentinizing aqueous fluids at low P-T conditions (stage 6, Fig. 12). Consistent with dolomite formation at the time of garnet formation (chapter "Dolomite formation from crust-derived …."), calcite-brucite intergrowths after dolomite predominate in serpentinized fine-grained mylonitic peridotites that once equilibrated in the garnet stability field. This is in agreement with the suggested clockwise exhumation path of the UZ rocks (Nimis and Morten, 2000; Tumiati et al., 2003), where coexisting hornblende + dolomite become instable at pressures < 1.5 GPa and temperatures ≤ 700°C (Nimis and Morten, 2000) while antigorite stabilizes (Fig. 12). In contrast, the preservation of interstitial discrete dolomite in some garnet-bearing fine-grained peridotites is attributed to the lack of serpentinization of these samples and the rapid P-T decrease during exhumation. This would be consistent with the Late-Carboniferous fast exhumation of the UZ mélange (Ranalli et al., 2005) and the assumption that rapid exhumation might have hampered slow dolomite-consuming silicate-carbonate reactions (Berg, 1986), in particular in the absence of catalyzing fluids. This also explains the occasional preservation of dolomite inclusions in crack-free host minerals, even in highly-serpentinized samples that contain calcite-brucite intergrowths related to serpentinization. The breakdown of dolomite into periclase + calcite symplectites, according to the reaction dolomite = calcite + periclase + CO_2, was observed in high-pressure garnet-peridotites (Yang et al., 1993), in mantle-derived xenoliths (Berg, 1986) and in marbles (Goldsmith, 1980). In the latter case, subsequent hydration of periclase lead to formation of brucite (Berg, 1986). This reaction sequence has been also suggested for other dolomite marbles where brucite has a spherical shape that has been interpreted to record the primary cubic periclase structure (Müller et al., 2009). The acicular habit of brucite within the calcite-brucite intergrowths in UZ peridotites reflects its trigonal crystal structure, and thus, brucite cannot be interpreted to be pseudomorphic after periclase. This is in agreement with the overlap of the UZ exhumation path (Nimis and Morten, 2000; Tumiati et al., 2003) with the brucite stability field given by the P-T curve for brucite-periclase equilibrium (Fig. 12) experimentally determined by Schramke et al. (1982). In the temperature range for UZ exhumation (decreasing from ~ 900°C), brucite forms even at decreasing water fugacities (Schramke et al., 1982) in a low-pressure range (0.1 to 2.0 GPa). This supports the inference that dedolomitization and carbon release in the UZ peridotites are caused by late low-P-T fluid infiltration inducing serpentinization (stage 6, Fig. 12) and direct formation of calcite-brucite intergrowths according to the reaction $CaMg(CO_3)_2 + H_2O \rightarrow CaCO_3 + Mg(OH)_2 + CO_2$. The occasional occurrence of dolomite grains embedded in the serpentine mesh texture (Fig. 7c) in samples containing calcite-brucite intergrowths might indicate infiltration by serpentinizing aqueous fluids while the mantle was still in the dolomite stability field and/or that dolomite which formed at high-pressure conditions (stage 2) persists metastably. Extrapolation of dolomite stability from experimentally determined conditions (Tumiati et al., 2013) to lower pressure and temperature (Fig. 12; area below 850°C) shows that dolomite might be stable at P-T conditions of antigorite stability, probably below 700°C during the UZ exhumation path.

Fate of carbon during dedolomitization and carbon recycling in collisional settings

The fine magnesite + serpentine veinlets with sharp boundaries crosscutting the ultramafic mineral assemblage (Fig. 11f) are interpreted as fracture fillings. Magnesite in these veinlets probably precipitated from a near-surface COH-fluid. This process has been previously suggested also for hydrothermal magnesite veins in serpentinites (e.g., Ghoneim et al., 2003) and is similar to the reaction path leading to listwanite formation in peridotites and serpentinites (e.g., Hansen et al., 2005; Power et al., 2013; Zhang et al., 2015): magnesite precipitates as fracture filling from fluids at the expense of serpentine minerals at a time after the serpentinization process, as discussed earlier for magnesite veins in samples SBB2F and KoD9 (chapter "Formation of retrograde magnesite"). Calcite veinlets in some coarse-grained samples cutting the ultramafic minerals may also be fracture fillings. In contrast, the fine calcite veinlets and patches in serpentinized fine-grained peridotites, rather than representing late fracture fillings, are suggested to be related to serpentinization as they are embedded within the serpentine mesh texture and therein often related to the calcite-brucite intergrowths. The close spatial relationship between calcite veinlets and magnetite within the serpentine veins reveals that the serpentinizing fluid was carbon-bearing. Although the source of carbon in this fluid is presently unconstrained, it may be speculated that dedolomitization, which was likely caused by fluid ingress, led to release of a mobile carbon species into the fluid (i.e. $CaMg(CO_3)_2 + H_2O \rightarrow CaCO_3 + Mg(OH)_2 + CO_2$). This would have enabled *in-situ* formation of secondary carbonate generations, now observed as veins (Fig. 11c, d). The lack of dedolomitization products in the majority of the coarse-grained peridotites, yet presence of calcite veinlets in some of these samples, is here taken to reflect local variations in the volume and carbon content (e.g., CO_2/H_2O) of the fluid. While the ultimate fate of the carbon released by dedolomitization remains unclear, multiple pieces of evidence suggest that the supra-subduction zone peridotitic mantle from the UZ largely acted as an efficient carbon trap: (1) Preservation of an early generation of discrete dolomite grains dating from the high-temperature mantle wedge stage, (2) additional generation of dolomite during interaction of supra-subduction zone mantle with fluids derived from the subducting continental crust, and, (3) breakdown of dolomite into calcite-brucite intergrowths, with attendant release of a carbon species that may have precipitated secondary carbonate minerals in veins and veinlets elsewhere as a function of P-T-X. Carbon fixation at the slab-wedge interface has been documented also in subduction zones involving oceanic slabs (Piccoli et al., 2016; Scambelluri et al., 2016).

SUMMARY AND CONCLUSIONS

The occurrences of different carbonate phases in various textural settings in the peridotites of the UZ indicate multi-stage carbonation and carbonate breakdown and may be linked to particular petrologic processes affecting the mantle wedge peridotite during the UZ tectonometamorphic evolution. At each stage of carbonate formation from COH-fluids, the composition of the fluid (e.g., X_{CO2}) controls the precipitation of particular carbonate phases making it difficult to estimate P-T conditions from a petrographical point of view only. Nevertheless, for the UZ peridotites, different stages of carbonate formation and breakdown can be identified and related to changing P-T conditions, depending on the presence or absence of fluids that are able to catalyze prograde or retrograde reactions:

1) An early generation of dolomite formed in the high-temperature spinel-stability field (stage 1). This is evidenced by euhedral grains of dolomite and calcite-brucite intergrowths in primary coarse spinel surrounded by garnet. The liquids responsible for dolomite formation may have been mafic carbonated melts produced in deeper parts of the subduction zone.
2) Dolomite and hydrous phases, such as pargasitic amphibole and apatite, are suggested to have formed from a H_2O-CO_2-mixed aqueous fluid released by the subducting continental slab in the garnet-stability field (~ 1.9 GPa, ≥ 900°C) during migmatization of host crustal rocks at 330 Ma (stage 2). Petrographic evidence for this includes euhedral discrete dolomite grains, often associated with and occasionally included in garnet, amphibole, apatite and olivine, exclusively in fine-grained non-serpentinized garnet-amphibole peridotites.
3) Local injection of a CO_2-rich aqueous fluid may have caused the formation of coexisting dolomite + magnesite outside garnet stability at ~ 2.0 GPa and ~ 850°C (stage 3), as suggested by associated interstitial anhedral dolomite and magnesite associated with amphibole in non-serpentinized coarse-grained garnet-free peridotite.
4) After high-pressure dolomite formation (stage 2) and prior to low-temperature serpentinization, CO_2-rich aqueous fluids locally caused the formation of veins and anhedral interstitial dolomite + amphibole (stage 4). This event is similar to stage 3 but takes place outside magnesite stability and is inferred from the observation of distinct veins consisting of anhedral dolomite grains associated with amphibole ± serpentine, crosscutting the peridotite matrix.
5) Retrograde magnesite formed in the antigorite stability field (≤ 730°C and ≤ 1.6 GPa) together with serpentine from an aqueous COH-fluid (stage 5), as indicated by an anhedral magnesite aggregate related to magnesite veinlets in garnet-free serpentinized fine-grained peridotite and therein texturally associated with serpentine.
6) During low-pressure/temperature serpentinization, dolomite decomposed into finely intergrown calcite + brucite due to interaction with H_2O-rich fluids (stage 6). This is evidenced by pseudomorphs after dolomite and the close spatial relationship of the intergrowths to serpentinization products. A carbon species was likely released during the process, which may have precipitated carbonates in veins and veinlets at appropriate P-T-X conditions, as observed ubiquitously in both fine-grained garnet-free and garnet-bearing peridotites, as well as in coarse-grained garnet-free peridotites.
7) Carbon-bearing aqueous near-surface fluids triggered syn- or post-serpentinization formation of veins in pre-existing pathways (e.g., cracks), consisting of further serpentine + magnesite and/or calcite.

Considering the stability of the various carbonates and coexisting silicate minerals, we suggest that the P-T conditions for carbonate formation in the UZ peridotites from aqueous COH-fluids could only be achieved in the supra-subduction zone mantle wedge close to the continental slab (Fig. 13). In contrast, carbonate formation in peridotites in the hot wedge, farther from the slab, could occur only from fluid and/or melts possibly originating from the deeper continental or preceding oceanic slab. A portion of the carbon released to the serpentinizing fluid causing dolomite breakdown may have escaped the system. However, overall, the ubiquity of carbonates in a variety of textural settings in the UZ peridotites, from discrete dolomite grains to vein-associated carbonates, and likely formed from a variety of liquids during several tectonometamorphic stages in the rocks' evolution, suggests that the supra-subduction zone mantle in continental settings represents an efficient carbon trap.

ACKNOWLEDGEMENTS

BF is deeply grateful to the authorities and people in Rumo (Trentino, Italy) as well as to a diligent assistant for enthusiastic help and advice during the field and sampling campaign. Giorgio Gasparotto is thanked for support at the SEM at the University of Bologna and Bruce Idleman is thanked for support and advice during SEM work at Lehigh University. Jürgen Konzett and Peter Tropper are thanked for assistance with SEM imaging at the University of Innsbruck. Gray E. Bebout kindly supported BF's stay at Lehigh University. We thank the University of Bologna and the Autonome Provinz Bozen - Südtirol for financial support and Alberto Vitale Brovarone and an anonymous reviewer for their constructive criticisms and two anonymous reviewers for their valuable comments on an earlier version of this manuscript.

REFERENCES

Ague J.J. and Nicolescu S., 2014. Carbon dioxide released from subduction zones by fluid-mediated reactions. Nat. Geosci., 7: 355-360.

Bebout G.E., 1996. Volatile transfer and recycling at convergent margins: mass-balance and insights from high-P/T metamorphic rocks. In: G.E. Bebout, D.W. Scholl, S.H. Kirby and J.P. Platt (Eds.), Subduction top to bottom. Am. Geophys. Union, Washington, D.C., p. 179-193.

Berg G.W., 1986. Evidence for carbonate in the mantle. Nature, 324: 50-51.

Braga R. and Sapienza G.T., 2007. The retrograde evolution of a dolomite-bearing hydrous peridotite from the Ulten Zone (Italian Alps). GeoActa, 6: 37-45.

Canil D., 1990. Experimental study bearing on the absence of carbonate in mantle-derived xenoliths. Geology, 18: 1011-1013.

Carswell D.A. and Van Roermund H.L.M., 2005. On multi-phase mineral inclusions associated with microdiamond formation in mantle-derived peridotite lens at Bardane on Fjørtoft, west Norway. Eur. J. Mineral., 17: 31-42.

Eggler D.H., 1978. Stability of dolomite in a hydrous mantle, with implications for the mantle solidus. Geology, 6: 397-400.

Eggler D.H., Kushiro I. and Holloway J.R., 1979. Free energies of decarbonation reactions at mantle pressures: I. Stability of the assemblage forsterite-enstatite-magnesite in the system MgO-SiO_2-CO_Z-H_2O to 60 kbar. Am. Mineral., 64: 288-293.

Facq S., Daniel I., Montagnac G., Cardon H. and Sverjensky D., 2014. *In situ* Raman study and thermodynamic model of aqueous carbonate speciation in equilibrium with aragonite under subduction zone conditions. Geochim. Cosmochim. Acta, 132: 375-390.

Ferrando S., Groppo C., Frezzotti M.L., Castelli D. and Proyer A., 2017. Dissolving dolomite in a stable UHP mineral assemblage: Evidence from Cal-Dol marbles of the Dora-Maira Massif (Italian Western Alps). Am. Mineral., 102: 42-60.

Frezzotti M.L. and Ferrando S., 2015. The chemical behaviour of fluids released during deep subduction based on fluid inclusions. Am. Mineral., 100: 352-377.

Frezzotti M.L., Selverstone J., Sharp Z.D. and Compagnoni R., 2011. Carbonate dissolution during subduction revealed by diamond-bearing rocks from the Alps. Nat. Geosci., 4: 703-706.

Fumagalli P. and Poli S., 2005. Experimentally determined phase relations in hydrous peridotites to 6.5 GPa and their consequences on the dynamics of subduction zones. J. Petrol., 46: 555-578.

Ghoneim M.F., Salem L.A. and Hamdy M.M., 2003. Origin of magnesite veins in serpentinites from Mount El-Rubshi and Mount El-Maiyit, Eastern desert, Egypt. Arch. Mineral., 54: 41-63.

Godard G. and Martin S., 2000. Petrogenesis of kelyphites in garnet peridotites: a case study from the Ulten Zone peridotites, Italian Alps. J. Geodyn., 30: 117-145.

Godard G., Martin S., Prosser G., Kienast J.R. and Morten L., 1996. Variscan migmatites, eclogites and garnet-peridotites of the Ulten Zone, Eastern Austroalpine system. Tectonophysics, 259: 313-341.

Goldsmith J.R., 1980. Thermal stability of dolomite at high temperatures and pressures. J. Geophys. Res., 85: 6949-6954.

Green D.H. and Wallace M.E., 1988. Mantle metasomatism by ephemeral carbonatite melts. Nature, 336: 459-462.

Green T.H., Adam J. and Sie S.H., 1992. Trace element partitioning between silicate minerals and carbonatite at 25 kbar and application to mantle metasomatism. Miner. Petrol., 46: 179-184.

Hansen L.D., Dipple G.M., Gordon T.M. and Kellet D.A., 2005. Carbonated serpentinite (listwanite) at Atlin, British Columbia: a geological analogue to carbon dioxide sequestration. Can. Mineral., 43: 225-239.

Hauzenberger C.A., Höller W. and Hoinkes G., 1996. Transition from eclogite to amphibolite-facies metamorphism in the Austroalpine Ulten Zone. Miner. Petrol., 58: 111-130.

Ionov D.A., 1998. Trace element composition of mantle-derived carbonates and coexisting phases in peridotite xenoliths from alkali basalts. J. Petrol., 39: 1931-1941.

Ionov D.A., Dupuy C., O'Reilly S.Y., Kopylova M.G. and Genshaft Y.S., 1993. Carbonated peridotite xenoliths from Spitsbergen: implications for trace element signature of mantle carbonate metasomatism. Earth Planet. Sci. Lett., 119: 283-297.

Ionov D.A., O'Reilly S.Y., Genshaft Y.S. and Kopylova M.G., 1996. Carbonate-bearing mantle peridotite xenoliths from Spitsbergen: phase relationships, mineral compositions and trace-element residence. Contrib. Mineral. Petr., 125: 375-392.

Jenkins D.M. and Newton R.C., 1979. Experimental determination of the spinel peridotite to garnet peridotite inversion at 900° C and 1,000° C in the system CaO-MgO-Al_2O_3-SiO_2, and at 900° C with natural garnet and olivine. Contrib. Mineral. Petr., 68: 407-419.

Kerrick D.M. and Connolly J.A.D., 1998. Subduction of ophicarbonates and recycling of CO_2 and H_2O. Geology, 26: 375-378.

Kerrick D.M. and Connolly J.A.D., 2001. Metamorphic devolatilization of subducted marine sediments and the transport of volatiles into the Earth's mantle. Nature, 411: 293-296.

Klemme S. and O'Neill H.St.C., 2000. The near-solidus transition from garnet lherzolite to spinel lherzolite. Contrib. Mineral. Petr., 138: 237-248.

Laurora A., Mazzucchelli M., Rivalenti G., Vannucci R., Zanetti A., Barbieri M.A. and Cingolani C.A., 2001. Metasomatism and melting in carbonated peridotite xenoliths from the mantle wedge: the Gobernador Gregores case (Southern Patagonia). J. Petrol., 42: 69-87.

Lee C-T., Rudnick R.L., McDonough W.F. and Horn I., 2000. Petrologic and geochemical investigation of carbonates in peridotite xenoliths from northeastern Tanzania. Contrib. Mineral. Petrol., 139: 470-484.

Malaspina N. and Tumiati, S., 2012. The role of C-O-H and oxygen fugacity in subduction-zone garnet peridotites. Eur. J. Mineral., 24: 607-618.

Manning, C.E., 2004. The chemistry of subduction-zone fluids. Earth Planet. Sci. Lett., 223: 1-16.

Manning C.E., Shock E.L. and Sverjensky D.A., 2013. The chemistry of carbon in aqueous fluids at crustal and upper-mantle conditions: experimental and theoretical constraints. Rev. Mineral. Geochem., 75: 109-148.

Marocchi M., Hermann J., Morten L., 2007. Evidence for multistage metasomatism of chlorite-amphibole peridotites (Ulten Zone, Italy): Constraints from trace element compositions of hydrous phases. Lithos, 99: 85-104.

Marocchi M., Mair V., Tropper P. and Bargossi G.M., 2009. Metasomatic reaction bands at the Mt. Hochwart gneiss-peridotite contact (Ulten Zone, Italy): insights into fluid-rock interaction in subduction zones. Miner. Petrol., 95: 251-272.

Martin S., Godard G., Prosser G., Schiavo A., Bernoulli D. and Ranalli, G., 1998. Evolution of the deep crust at the junction Austroalpine/Southalpine: the Tonale Nappe. Mem. Sci. Geol. (Padova), 50: 3-50.

Martin S., Morten L. and Prosser G., 1993. Metamorphic and structural evolution of the Spl- to Grt-peridotites and surrounding basement rocks from the Nonsberg area. In: L. Morten (Ed.), Italian eclogites and related rocks. Rend. Accad. Naz. Quaranta, 13: 237-251.

Molina J.F. and Poli S., 2000. Carbonate stability and fluid compositions in subducted oceanic crust: an experimental study on H_2O-CO_2-bearing basalts. Earth Planet. Sci. Lett., 176: 295-310.

Morten L. and Obata M., 1983. Possible high-temperature origin of pyroxenite lenses within garnet peridotite, Northern Italy. Bull. Minéral., 106: 775-780.

Morten L., Bargossi G.M. and Bargossi F., 1976. Notizie preliminari sulle metamorfiti della Val di Rumo, Val di Non, Trento. Mineral. Petrogr. Acta, 21: 137-144.

Müller T., Baumgartner L.P., Foster Jr. C.T. and Bowman J.R., 2009. Crystal size distribution of periclase in contact metamorphic dolomite marbles from Southern Adamello Massif, Italy. J. Petrol., 50: 451-465.

Naemura K., Hirajima T. and Svojtka M., 2009. The pressure-temperature path and the origin of phlogopite in spinel-garnet peridotites from the Blanský Les Massif of the Moldanubian Zone, Czech Republic. J. Petrol., 50: 1795-1827.

Nimis P. and Morten L., 2000. P-T evolution of "crustal" garnet peridotites and included pyroxenites from Nonsberg area (Upper Austroalpine), NE Italy: from the wedge to the slab. J. Geodyn., 30: 93-115.

Obata M. and Morten L., 1987. Transformation of spinel lherzolite to garnet lherzolite in ultramafic lenses of the Austridic Crystalline Complex, Northern Italy. J. Petrol., 28: 599-623.

Piccoli F., Brovarone A.V., Beyssac O., Martinez I., Ague J.J. and Chaduteau C., 2016. Carbonation by fluid-rock interactions at high-pressure conditions: Implications for carbon cycling in subduction zones. Earth Planet. Sci. Lett., 445: 146-159.

Poli S., 2015. Carbon mobilized at shallow depths in subduction zones by carbonatitic liquids. Nat. Geosci., 8: 633-636.

Poli S., Franzolin E., Fumagalli P. and Crottini A., 2009. The transport of carbon and hydrogen in subducted oceanic crust: An experimental study to 5 GPa. Earth Planet. Sci. Lett., 278, 350-360.

Power I.M., Wilson S.A. and Dipple G.M., 2013. Serpentinite carbonation for CO_2 sequestration. Elements, 9: 115-121.

Rampone E. and Morten L., 2001. Records of crustal metasomatism in the garnet peridotites of the Ulten Zone (Upper Austroalpine, Eastern Alps). J. Petrol., 42: 207-219.

Ranalli G., Martin S. and Mahatsente R., 2005. Continental subduction and exhumation: an example from the Ulten Unit, Tonale Nappe, Eastern Austroalpine. In: D. Gapais, J.P. Brun and P.R. Cobbold (Eds.), Deformation mechanisms, rheology and tectonics: from minerals to the lithosphere. Geol. Soc. London Spec. Publ., 243: 159-174.

Sapienza G.T., Scambelluri M. and Braga, R., 2009. Dolomite-bearing orogenic garnet peridotites witness fluid-mediated carbon recycling in a mantle wedge (Ulten Zone, Eastern Alps, Italy). Contrib. Mineral. Petrol., 158: 401-420.

Scambelluri M. and Philippot P., 2001. Deep fluids in subduction zones. Lithos, 55: 213-227.

Scambelluri M., Bebout G.E., Belmonte D., Gilio M., Campomenosi N., Collins N. and Crispini L., 2016. Carbonation of subduction-zone serpentinite (high-pressure ophicarbonate; Ligurian Western Alps) and implications for the deep carbon cycling. Earth Planet. Sci. Lett., 441: 155-166.

Scambelluri M., Hermann J., Morten L. and Rampone E., 2006. Melt- versus fluid-induced metasomatism in spinel to garnet wedge peridotites (Ulten Zone, Eastern Italian Alps): clues from trace element and Li abundances. Contrib. Mineral. Petrol., 151: 372-394.

Schramke J.A., Kerrick D.M. and Blencoe J.G., 1982. Experimental determination of the brucite = periclase + water equilibrium with a new volumetric technique. Am. Mineral., 67: 269-276.

Shcheka S.S., Wiedenbeck M., Frost D.J. and Keppler H., 2006. Carbon solubility in mantle minerals. Earth Planet. Scl. Lett., 245: 730-742.

Timina T.Y., Kovyazin S.V. and Tomilenko A.A., 2012. The composition of melt and fluid inclusions in spinel of peridotite xenoliths from Avacha volcano (Kamchatka). Dokl. Earth Sci., 442: 115-119.

Tumiati S., Fumagalli P., Tiraboschi C. and Poli S., 2013. An experimental study on COH-bearing peridotite up to 3.2 GPa and implications for crust-mantle recycling. J. Petrol., 54: 453-479.

Tumiati S., Godard G., Martin S., Klötzli U. and Monticelli D., 2007. Fluid-controlled crustal metasomatism within a high-pressure subducted mélange (Mt. Hochwart, Eastern Italian Alps). Lithos, 94: 148-167.

Tumiati S., Godard G., Martin S., Nimis P., Mair V. and Boyer B., 2005. Dissakisite-(La) from the Ulten zone peridotite (Italian Eastern Alps): A new end-member of the epidote group. Am. Mineral., 90: 1177-1185.

Tumiati S., Thöni M., Nimis P., Martin S. and Mair V., 2003. Mantle-crust interactions during Variscan subduction in the Eastern Alps (Nonsberg-Ulten zone): geochronology and new petrological constraints. Earth Planet. Sci. Lett., 210: 509-526.

Whitney D.L and Evans B.W., 2010. Abbreviations for names of rock-forming minerals. Am. Mineral., 95: 185-187.

Wyllie P.J. and Huang W.L., 1975. Peridotite, kimberlite, and carbonatite explained in the system CaO-MgO-SiO_2-CO_2. Geology, 3: 621-624.

Yang J., Godard G., Kiénast J.R., Lu Y. and Sun J., 1993. Ultrahigh-pressure (60 kbar) magnesite-bearing garnet peridotites from Northeastern Jiangsu, China. J. Geol., 101: 541-554.

Zaccarini F., Stumpel E.F. and Garuti G., 2004. Zirconolite and Zr-Th-U minerals in chromitites of the Finero complex, Western Alps, Italy: evidence for carbonatite-type metasomatism in a subcontinental mantle plume. Can. Mineral., 42: 1825-1845.

Zanetti A., Mazzucchelli M., Rivalenti G. and Vannucci R., 1999. The Finero phlogopite-peridotite massif: an example of subduction-related metasomatism. Contrib. Mineral. Petrol., 134: 107-122.

Zhang L., Yang J., Robinson P.T., Xiong F., Chen Y., Lai S. and Chen M., 2015. Origin of listwanite in the Luobusa Ophiolite, Tibet, implications for chromite stability in hydrothermal systems. Acta Geol. Sin.-Engl., 89: 402-417.

Received, April 12, 2017
Accepted, June 22, 2017